

LEWIS DRAWING
1N-39
312067
P-70

NASA Contractor Report 185303

Materials With Periodic Internal Structure: Computation Based on Homogenization and Comparison With Experiment

S. Jansson, F.A. Leckie, E.T. Onat, and M.P. Ranaweera
*University of California
Santa Barbara, California*

October 1990

Prepared for
Lewis Research Center
Under Grant NAG3-894



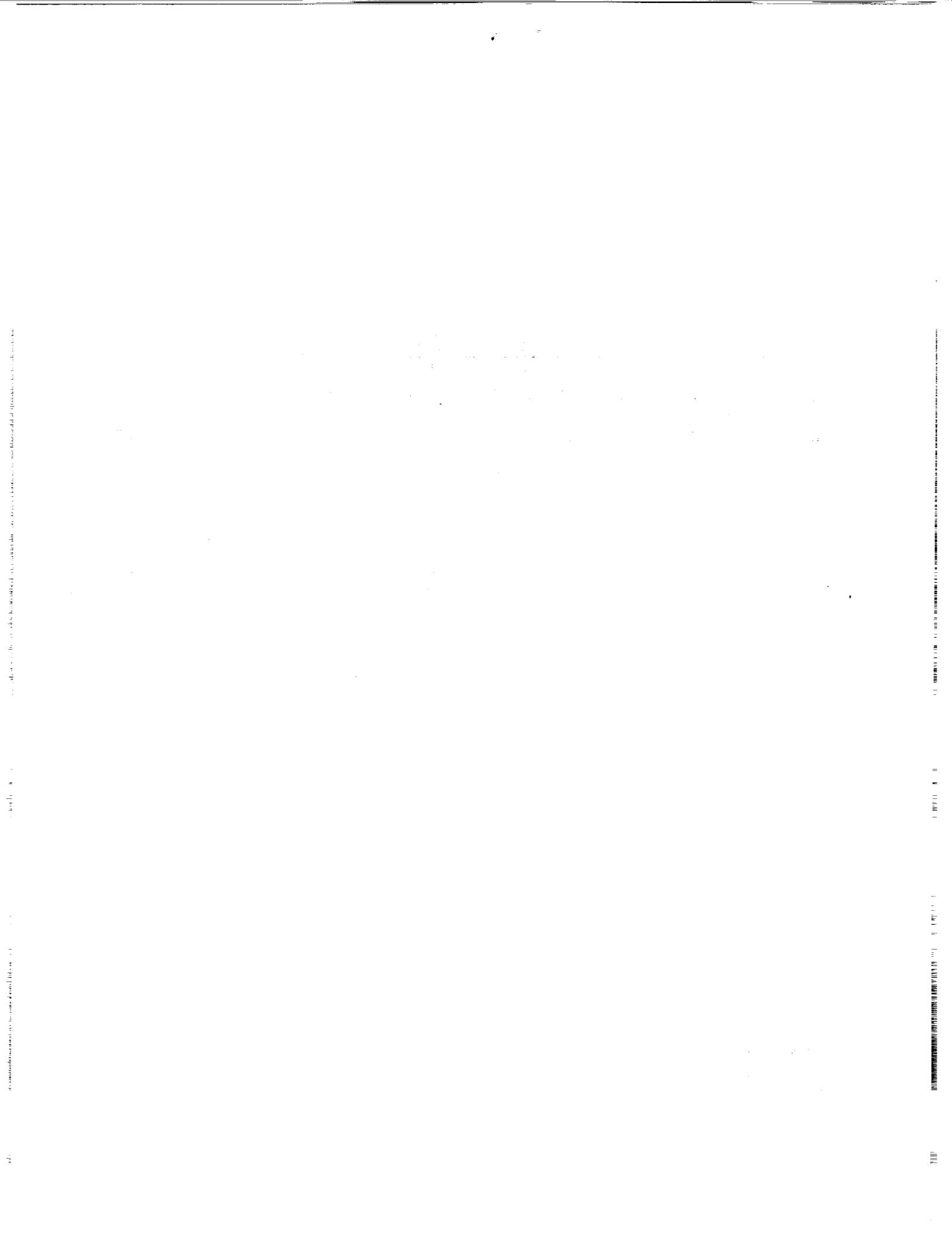
National Aeronautics and
Space Administration

(NASA-CR-185303) MATERIALS WITH PERIODIC
INTERNAL STRUCTURE: COMPUTATION BASED ON
HOMOGENIZATION AND COMPARISON WITH
EXPERIMENT Final Report (California Univ.)
70 p

N91-12117

Unclas
0312067

CSCL 20K G3/39



Materials with Periodic Internal Structure:[†] Computation Based on Homogenization and Comparison with Experiment

S. Jansson, F.A. Leckie, E.T. Onat, and M.P. Ranaweera

Abstract

The combination of thermal and mechanical loading expected in practice means that constitutive equations of metal matrix composites must be developed which deal with time-independent and time-dependent irreversible deformation. Also, the internal state of composites is extremely complicated which underlines the need to formulate macroscopic constitutive equations with a limited number of state variables which represent the internal state at the micro level. One available method for calculating the macro properties of composites in terms of the distribution and properties of the constituent materials is the method of homogenization whose formulation is based on the periodicity of the substructure of the composite.

In this study a homogenization procedure has been developed which lends itself to the use of the finite element procedure. The efficiency of these procedures, to determine the macroscopic properties of a composite system from its constituent properties, has been demonstrated utilizing an aluminum plate perforated by directionally oriented slits. The selection of this problem is based on the fact that, i) extensive experimental results exist, ii) the macroscopic response is highly anisotropic and iii) that the slits provide very high stress gradients (more severe than would normally be found in practice) which severely test the effectiveness of the computational procedures. Furthermore, both elastic and plastic properties have been investigated so that the application to practical systems with inelastic deformation should be able to proceed without difficulty. The effectiveness of the procedures have been rigorously checked against experimental results and with the predictions of approximate calculations. Using the computational results it is illustrated how macroscopic constitutive equations can be expressed in forms of the elastic and limit load behavior.

[†] Work funded under NASA Grant NAG3-894.

INTRODUCTION

The combination of thermal and mechanical loading expected in practice means that constitutive equations of metal matrix composites must be developed which deal with time-independent and time-dependent irreversible deformations. The so-called unified constitutive equations are likely to provide a good basis for the description of the matrix material but the combined effect of the matrix and reinforcing material remains to be determined. One available method for calculating the macro properties of composites in terms of the properties and distribution of the constituent materials is the method of homogenization whose formulation is based on periodicity of the substructure of the composite. The method can coincide with the classical method of representing the substructure by a unit cell representation when conditions of symmetry are valid. However the advantages of the method of homogenization are that its formulation allows it to be used when symmetry no longer applies, offers the possibility of determining the stress and strain fields at the microscopic level and provides a formal derivation of unit cell representation. By following this procedure failure criteria can be introduced into the calculations for the constituents and interfaces which are based on micro-mechanical models. Studies which establish the macro-mechanical properties of the composite from the properties of the constituents afford the opportunity of directly designing composite material properties. When studying component behavior however it is more convenient to use constitutive equations which describe the macroscopic properties of the material. Such constitutive equations can be developed from the results of mechanical tests. However it is also possible to use homogenization procedures to simulate the experimental program and provide the results from which constitutive equations can be formulated.

In this study a convenient form of this homogenization procedure has been developed which lends itself to the use of the finite element procedure. The procedure is based on the assumption that stress fields vary slowly from one homologous point to another. In the absence of point loads and away from boundaries we expect this assumption to be valid. However, this expectation is not fulfilled in the vicinity of stress-free boundaries or in the vicinity of cracks where stress gradients are large. For nonlinear and inelastic problems

localization of deformation is a possibility. If localization takes place in a region of a few cells then homogenization may not be applicable because macro-strain gradients are large. However, the procedure may still be valid provided localization occurs over many cells (twenty say).

To illustrate the application of the procedure a plate system has been selected for which extensive experimental results exist. The system consists of an aluminum plate perforated by directionally oriented slits. In addition to providing a basis of comparison for the predictions of the calculations, the stress concentration factors are high and provide a severe test on the effectiveness of the computational procedures. Finally the anisotropic character is pronounced and is difficult to represent at the macroscopic level.

A further study given in a subsequent report is the prediction of the macroscopic properties of a metal matrix composite using the known properties of the matrix and the fiber. An experimental program has also been completed so that comparison with the computational results can be made. This study is particularly important since if the predictions of the calculations can be verified then the procedure can replace the difficult test program which is often limited by the shortage of material.

2. THE HOMOGENIZATION PROCEDURE

2.1 Formulation

Consider a structure composed of a periodically inhomogeneous material (Fig. 2.1). The material is linear elastic and locally isotropic. For further simplicity assume that the inhomogeneity is planar so that the the Lamé constants of the material depend only on the transverse coordinates x_1 and x_2 as follows:

$$\mu(x + d e_\alpha) = \mu(x), \quad x \in \mathbb{R}^2, \quad \alpha = 1, 2 \quad (2.1)$$

where e_1 and e_2 are the first two unit vectors of the rectangular frame and x lies in their span (similar equation for the other Lamé constant λ).

We shall be concerned here with **small plane deformations** and rotations which

in the present case can take place in the absence of the stress components σ_{13} and σ_{23} and we shall regard the material as infinite and two dimensional. It is then useful to think of the structure as a two dimensional sub-set B of the material shown in Fig. 2.1 where the material is composed of the copies of a unit cell of square cross section which is of size d and contains, say, a hard fiber of circular cross section.

The elastic structure B is subject to given surface tractions T on ∂B_T and given displacements U on ∂B_U . It is required to determine the resulting fields $u_i(x)$, $\epsilon_{ij}(x)$, and $\sigma_j(x)$ of displacement, strain and stress respectively (Fig. 2.1).

If the characteristic lengths of this elasticity problem (the diameter D of the body, the minimum radius of curvature of the concave parts of the boundary ∂B of the body, the "wave" lengths l_T and l_U associated with surface tractions and displacements, etc.) are much larger than the cell size d , then one expects that the solution of the above problem of elasticity would exhibit certain properties. A careful statement of these properties will require a family of decreasing cell size so that statements can be made about the material properties as d/D tends to zero. Thus following the French school⁽¹⁾ we will define the Lamé constants of the material with cell size d as $\mu^{(d)}(x) = \mu^{(1)}(x/d)$ where $\mu^{(1)}$ is a one-periodic continuous function.

For a discussion of the anticipated properties of the elasticity problem of Fig. 2.1 it is desirable to consider a generic nine-cell sub-domain within the body (Fig. 2.2a). The deformed shape of this domain may be as shown in Fig. 2.2b. Due to inhomogeneity of the material, the stress fields within a cell will exhibit variations so that $\sigma(P_1)$, the stress at P_1 , is likely to be quite different from $\sigma(Q_1)$ and the deformed shape of the boundary of the cell will exhibit a waviness of size d . However, if one considers three homologous points P_1 , P_2 and P_3 within the sub-domain (these points have the same coordinates in respective cell coordinate frames), then $\sigma(P_1)$, $\sigma(P_2)$ and $\sigma(P_3)$ will differ from each other only a little. More precisely, say

$$\|\sigma(P_1) - \sigma(P_2)\| / \langle \|\sigma\| \rangle \ll 1$$

In view of the above cited expectations, the deformed state of the nine-cell sub-domain can be approximated by the one shown in Fig. 2.2c which is macroscopically homogeneous. Thus, in this figure, the same stress will be obtained in homologous locations P_i' which now lie on a straight line and, therefore, the new locations A'B'C'C' of the cell-corners will define a parallelogram.

Reflection will show that the displacement field $V_i(x)$ associated with the macroscopically homogeneous field shown in Fig. 2.2c will be of the following form in the case of small plane deformations and rotations

$$V_i(x) = E_{ij} x_j + \Omega_{ij} x_j, \quad i, j = 1, 2 \quad (2.2)$$

where the usual summation convention is used and E_{ij} and Ω_{ij} are the components of the constant infinitesimal tensors of strain and rotation that determine the shape and orientation of the parallelogram A'B'C'D'. Here, $V_i(x)$ are the components of a d-periodic and continuous displacement field,

$$V_i(x + d e_j) = V_i(x) \quad (2.3)$$

The strains created by the field (2.2) are

$$\varepsilon_{ij}(x) = \frac{1}{2}(V_{i,j} + V_{j,i}) + E_{ij} \quad (2.4)$$

where comma denotes partial differential in the usual way.

It will be noted that on account of the periodicity of V_i the average of ε_{ij} over a cell is equal to E_{ij} :

$$\langle \varepsilon_{ij} \rangle_c = E_{ij} \quad (2.5)$$

where the brackets indicate the average, over a cell, of the bracketed quantity.

The stresses created by the above strains will satisfy the equations of equilibrium:

$$\frac{\partial}{\partial x_i} \left\{ C_{ijkl}(x) \left[\frac{1}{2} (V_{k,l} + V_{l,k}) \right] \right\} = 0 \quad (2.6)$$

where $C_{ijkl}(x)$ are the d-periodic moduli of elasticity

$$C_{ijkl}(x) = \mu(x)(\delta_{ik}\delta_{jl} + \delta_{il}\delta_{jk}) + \lambda(x)\delta_{ijkl}.$$

It is known that, when combined with the periodicity of continuity of $V_i(x)$, Eqn. (2.6) constitutes a well-posed linear problem defined over the interior D_c of a cell for the determination of $V_i(x)$ as functions of the prescribed constant average strain components E_{ij} .

In view of the linearity of the problem, and with the arbitrary but permissible choice that $V_i(x) = 0$ on the corners of cells, (2.6) has the unique solution

$$V_i(x) = g_{ijk}(x) E_{jk} \quad (2.7)$$

where the functions $g_{ijk}(x)$ follow uniquely from the elastic moduli $C(x)$ of the material.

Note that

$$g_{ijk} = g_{ikj}$$

and there are six such d-periodic functions. In this report the functions $g_{ijk}(x)$ are determined by finite element methods.

Combining (2.7) with (2.4) and the Hooke's law, we find the macrostrains and stresses created by the constant average strain E_{kl} :

$$\varepsilon_{ij}(x) = E_{ij} + 1/2(g_{ikl,j}(x) + g_{jkl,i}(x)) E_{kl},$$

$$\sigma_{ij}(x) = H_{ijkl}(x) E_{kl} \quad (2.8)$$

where

$$H_{ijkl}(x) = [C_{ijkl}(x) + C_{ijmn}(x) g_{mkl, n}(x)].$$

From the expression (2.7) it can be deduced that g_{rkl} are of the order d and therefore $g_{mkl, n}$ are of the order "one" [2,3].

Note that $H_{ijkl}(x)$ are d -periodic. It follows from the equations of equilibrium and from the fact that E_{kl} are arbitrary constants that

$$H_{ijkl}(x),_{,j} = [C_{ijkl}(x) + C_{ijmn}(x) g_{mkl, n}(x)],_{,j} = 0 \quad (2.9)$$

It will be observed that (2.9) could be thought as providing six equations for the determination of the function $g_{mkl}(x)$ and is equivalent to (2.6).

By averaging, we obtain from (2.8)

$$\Sigma_{ij} = K_{ijkl} E_{kl} \quad (2.10)$$

where

$$\Sigma_{ij} = \langle \sigma_{ij} \rangle_c \text{ and } K_{ijkl} = \langle H_{ijkl}(x) \rangle_c \quad (2.11)$$

and brackets indicate, as before, the average of the bracketed quantity over a cell.

We refer to Σ_{ij} as the average stress or the macro-stress. K_{ijkl} are the components of the constant effective moduli of the problem. It can be shown by using (2.9) that K_{ijkl} inherit the symmetry properties of C_{ijkl} exhibited before. Moreover it can also be shown that for the family of the materials considered here K_{ijkl} are independent of the cell size d !

It is noted that finite element techniques can and have been applied (cf. [1]) to a single cell to obtain approximations to the functions $g_{ijk}(x)$, $H_{ijkl}(x)$ and, hence to the effective

moduli K_{ijkl} .

After this initial step which is independent of the body and the loads it carries and produces the effective moduli and the important relationships (2.7) and (2.8), we are ready to discuss the remaining steps of the homogenization program which leads to an approximate solution of the problem of finding the fields of displacement and stress within the body B.

2.2 Homogenized Body, Macro-Stresses and Strains

The structure B is now thought of as composed of a homogeneous elastic material which possesses the effective moduli K obtained in Section 2.1. The distributions $\Sigma(x)$ and $E(x)$ of the macro- or average-stresses and strains are then found by solving a classical boundary value problem of elasto-statics over B with the boundary conditions of the original problem (Fig. (2.1)):

$$\begin{aligned} \Sigma_{ij} n_j &= T_i(x) & \text{on } \partial B_F \\ U_i &= u_i(x) & \text{on } \partial B_U \end{aligned} \quad (2.12)$$

where $U_i(x)$ are the displacements that give rise to the distribution $E_{ij}(x)$ of the macro-strains over the body.

The distribution of the micro stresses and strains within the body can then be determined in the following way.

In view of (2.7) and (2.2) the displacement field \hat{u}_i is offered as an approximation to the actual field $u_i(x)$ of the very first problem of Fig. 2.1):

$$\hat{u}_i(x) = U_i(x) + g_{ijk}(x)E_{jk}(x) \quad (2.13)$$

where $U_i(x)$ and $E_{jk}(x)$ are the fields of displacement and strain in the homogenized body and the functions $g_{ijk}(x)$ were obtained in the first step of the homogenization program.

The above displacement field is kinematically acceptable everywhere except on the boundary ∂B_U where the second term on the r.h. of the above equation and therefore the

difference ($\hat{u}_i - U_i$) will, in general, not vanish (cf. Fig. (2.2b)).

Let ρ_i^u denote the deficit in displacements on ∂B_u :

$$\rho_i^u = \hat{u}_i(x) - u_i(x) = g_{ijk}(x)E_{jk}(x) \quad (2.14)$$

We recall that g_{ijk} is of the order of d and therefore we expect that the steps needed to be taken to remove this deficit will cause only local changes in the fields introduced above. Errors shall be discussed later.

The strains created by the displacement field $\hat{u}_i(x)$ are then

$$\hat{\epsilon}_{ij}(x) = E_{ij}(x) + 1/2(g_{ikl,j} + g_{jkl,i})E_{kl}(x) + 1/2(g_{ikl}E_{kl,j} + g_{jkl}E_{kl,i}) \quad (2.15)$$

which give rise to the stress field

$$\hat{\sigma}_{ij}(x) = C_{ijkl}(x)\hat{\epsilon}_{kl}(x), \quad x \in B \quad (2.16)$$

In view of the developments which led to (2.8) and (2.11), the above equation becomes

$$\hat{\sigma}_{ij}(x) = H_{ijkl}(x)E_{kl}(x) + [C_{ijkl}(x)g_{kmn}(x)E_{mn,l}(x)] \quad (2.17)$$

where as before

$$H_{ijkl}(x) = [C_{ijkl}(x) + C_{ijmn}(x)g_{mkl,n}(x)].$$

We note that the first term on the right hand side of (17) is of the "order" of the macro-stresses $\Sigma_{ij}(x)$ and coincides with the leading term of the asymptotic expansion used in the work of Duvaut [2] for the stress components. We also observe that the second term in (2.17) is of the order of d/D .

2.3. Errors in Homogenization

It is a valid question to pose how close are the fields $\hat{u}_i(x)$ and $\hat{\sigma}_{ij}(x)$ obtained by the homogenization program to those occurring in the heterogeneous medium.

It was shown in [2] that

$$\Sigma_{ij}(x) - H_{ijkl}(x) E_{kl}(x) \rightarrow 0 \quad (2.18)$$

as $d/D \rightarrow 0$.

This important result does not, of course, imply that the above difference tends to zero everywhere. Indeed, as we shall see, on ∂B_F the difference is not zero, in general, and remains so as d/D tends to zero. Moreover when d/D is finite but still small there may be other parts of the body where the above difference may be unacceptably large (cf. Fig. 2.2d).

The starting point in the construction of the approximate fields was the choice of the displacements $\hat{u}_i(x)$. It was demonstrated that this field fails to satisfy the b.c. on ∂B_U and it is now studied whether the stress field $\hat{\sigma}_{ij}(x)$ derived from it satisfies the requirements of equilibrium.

Consider first the equilibrium of the material elements adjacent to the boundary ∂B_F of the body where surface tractions are prescribed. Equilibrium demands that the vector

$$\hat{\sigma}_{ij}(x)n_j(x) - T_i(x)$$

should vanish on ∂B_F where $n_j(x)$ are the components of the unit outward normal to the boundary. Since $\hat{\sigma}_{ij}(x)$ exhibits, in general, spatial variations over the cell due the inhomogeneity of the material and $T_i(x)$ is, by assumption (cf. Fig. 2.1), a function of long wave length the above difference will not, in general, be zero (cf. Fig. 2.2e).

This leads us to introduce the vector value function $\rho_i^{\dagger}(x)$ which measures the deficit in equilibrium on ∂B_F :

$$\rho_1^f(x) = \hat{\sigma}_{ij}(x)n_j(x) - T_i(x) \quad \text{on } \partial B_F \quad (2.19)$$

Note that in view of (2.12) the above equation can be written as

$$\rho_1^f(x) = (\hat{\sigma}_{ij}(x) - \Sigma_{ij}(x))n_j(x) \quad \text{on } \partial B_F \quad (2.20)$$

In the case shown in Fig. 2.3e $\max |\rho_2^f(x)|$ on the stress free boundary is independent of d and it is known from the numerical work reported later that it is of the order of the applied stress $\Sigma_{\alpha\alpha}$.

Similarly the deficit $r_i(x)$ in equilibrium in the interior B of the body is defined by considering the divergence of the stress field $\hat{\sigma}_{ij}(x)$:

$$r_i(x) = \hat{\sigma}_{ij,j}(x) \quad (2.21)$$

and using (2.17)

$$\begin{aligned} r_i(x) = & H_{ijkl}(x)_{,j} E_{kl}(x) + H_{ijkl}(x) E_{kl}(x)_{,j} \\ & + [C_{ijkl}(x) g_{kmn}(x) E_{mn,l}(x)]_{,j} \end{aligned}$$

The first term on the r.h. of the above vanishes by (2.9) so that

$$r_i(x) = H_{ijkl}(x) E_{kl}(x)_{,j} + [C_{ijkl}(x) g_{kmn}(x) E_{mn,l}(x)]_{,j} \quad (2.22)$$

We observe that each of the two terms on the right hand of (2.22) will be of the order of $\|\hat{\sigma}_{ij}(x)\|/D$ in the interior of the body B . However near a concave portion of the boundary ∂B the gradient of $E_{kl}(x)$ can be large so that a more refined estimation of $r_i(x)$ will be needed in such locations.

It is important to note that the solution of the boundary value problem for the

inhomogeneous elastic body B with the boundary conditions

$$\begin{aligned} u_i &= -\rho_i^U(x) && \text{on } \partial B_U \\ T_i &= -\rho_i^T(x) && \text{on } \partial B_T \end{aligned}$$

and subject to the body forces b_i (2.23)

$$b_i = -r_i(x) \quad \text{in } B$$

would provide the fields of displacement and stress which when added respectively to the fields $\hat{u}_i(x)$ and $\hat{\sigma}_{ij}(x)$ would produce the exact fields $u_i(x)$ and $\sigma_{ij}(x)$.

Clearly the problem of estimating errors in homogenization is equivalent to that of estimating the solution of (2.23). This leads us to the study of the deficits listed on the right hand of (2.23).

The specific example selected for illustration involves corrections for the deficit in equilibrium on ∂B_T . Consider first a reduced version of the elastostatics problem defined in (2.23). Let u_i and b_i vanish, but let T_i have the values given in (2.23). The question then arises about the displacements and stresses created in B by the surface tractions $-\rho_i^T(x)$ applied on ∂B_T ? The important result (2.18) of asymptotic analysis suggests that when d/D is small these correction fields must decay strongly from ∂B_T towards the interior of the body. The reason for this strong decay is a version of the de Saint Venant principle when applied to periodically inhomogeneous elastic bodies.

For this purpose consider the following integral

$$f(p_1, p_2) = \int_{p_2}^{p_1} (\hat{\sigma}_{i1}(x) - \Sigma_{i1}(x)) dx_2, \quad x_1 = p_1 \quad (2.24)$$

where the segment of integration which is of length d and parallel to the x_2 -axis is assumed to be on the boundary of B.

Note that if the point (p_1, p_2) were on ∂B_F and if x_1 were constant on the boundary then (2.24) would measure the resultant of $\rho_i^{\dagger}(x)$ over the side of a cell:

$$f(p_1, p_2) = \int_{p_2}^{p_2+d} \rho_i^{\dagger}(x) dx_2, \quad x_1 = p_1 \quad (2.25)$$

Now using (2.17) and (2.10), but neglecting terms of order d/D in (2.17), with the expansion

$$E_{kl}(p_1, x_2) \approx E_{kl}(p_1, p_2) + E_{kl,2}(p_1, p_2)(x_2 - p_2) + 1/2! E_{kl,22}(p_1, p_2)(x_2 - p_2)^2$$

(2.24) becomes

$$f(p_1, p_2) \approx \int_{p_2}^{p_2+d} (H_{i1kl}(p_1, x_2) - K_{i1kl}) [E_{kl}(p_1, p_2) + E_{kl,2}(p_1, p_2)(x_2 - p_2) + 1/2! E_{kl,22}(p_1, p_2)(x_2 - p_2)^2] dx_2 \quad (2.26)$$

Using (2.9) and (2.11) and the d -periodicity of $H(x)$ gives the result

$$\int_{p_2}^{p_2+d} (H_{i1kl}(p_1, x_2) - K_{i1kl}) dx_2 = 0 \quad (2.27)$$

so that

$$f(p_1, p_2) \approx \int_{p_2}^{p_2+d} (H_{i1kl}(p_1, x_2) - K_{i1kl}) [E_{kl,2}(p_1, p_2)(x_2 - p_2) + 1/2! E_{kl,22}(p_1, p_2)(x_2 - p_2)^2] dx_2 \quad (2.28)$$

This is an important result on various counts. First of all it shows that

$$f(p_1, p_2) \approx \kappa E_{kl,2}(p_1, p_2) O(d^2) \quad (2.29)$$

where κ is a constant which has the dimension of stress.

In the case where the boundary has a section parallel to the x_2 -axis (2.29) and (2.25) show that the resultant of the deficit $\rho_1^1(x)$ over a length d of the boundary is two orders of magnitude smaller than the local value of the deficit (which is of the order of the local macro-stress). Clearly the same result applies to those parts of the boundary that are parallel to the x_1 -axis.

Next consider the case when the boundary may intersect the cells "diagonally". For a study of this case consider a simply connected domain c in B and let δc be its boundary. Now consider the integral

$$\int_{\delta c} (\hat{\sigma}_{ij}(x) - \Sigma_{ij}(x)) n_j(x) ds$$

where $n_j(x)$ denotes the outward unit normal to the boundary.

It will prove useful in the sequel to observe from (2.21) and from the fact that $\Sigma_{ij}(x)$ satisfies equilibrium that

$$\int_{\delta c} (\hat{\sigma}_{ij}(x) - \Sigma_{ij}(x)) n_j(x) ds = \int_c r_i(x) dA \quad (2.30)$$

Choosing c as a square of size d and with sides parallel to the coordinate axes and by a repeated application of (2.28) using the fact that $H_{ijkl}(x)$ is d -periodic, it is found that

$$\int_{\delta c} (\hat{\sigma}_{ij}(x) - \Sigma_{ij}(x)) n_j(x) ds = \mu |E_{ij,1k}| O(d^3)$$

or equivalently (2.31)

$$\int_c \mathbf{r}_1(\mathbf{x}) dA = \mu |E_{ij,1k}| O(d^3)$$

where the constant μ has the dimension of stress and c denotes a cell size and oriented domain and the bars indicate a suitable norm. Hence the residual is of order d^3 but is also dependent on the second derivative of the strain field E_{ij} . Hence the errors are small provided the strain E_{ij} do not have larger gradients.

3. APPLICATION TO PLATE WITH ORIENTED CRACKS

The study by Litwka and Sawczuk [3] of the properties of plates perforated by periodically disposed slits is used as an example to study the effectiveness of the homogenization procedure. The example was selected because experimental data was available against which to test the predictions of the procedure. Furthermore, the shape and distribution of cracks is such that severe demands are made on the computations since the stress gradients within the unit elements are large in the vicinity of the slots.

A representative drawing of the perforated plate is shown in Fig. 3.1a and the dimensions of the cracks are given in Fig. 3.1b. The plates were made from an aluminum alloy whose stress/strain relationship is given in Fig. 3.2. The macro stress, macro strain relationships for the perforated plate for different values of the crack alignment are also shown in Fig. 3.2. The failure modes are reported by Litwka and Morzynska [4] and involve various forms of strain locations as illustrated in Fig. 3.3.

3.1 Loading and Boundary Conditions for Element

Following the procedures described in Section 2, the periodic element is of size $D = 10$ mm and the loading direction in relation to the direction of elongation of the cracks is defined by the angle α (Fig. 3.1b). The macro quantities are the stresses $\Sigma_x, \Sigma_y, \Sigma_{xy}$ and strains E_x, E_y, E_{xy} while the micro quantities are represented by $\sigma_x, \sigma_y, \tau_{xy}$ and $\epsilon_x, \epsilon_y, \gamma_{xy}$ respectively. The homogenization procedure was completed using finite element representation of quarter of the element as shown in Fig. 3.5. All the analysis was performed using the ABAQUS [5] system using the 8 node, isoparametric plane stress element CPS8. Incremental elastic/plastic calculations were performed using the Mises Yield Criterion in conjunction with an isotropic incremental hardening law for which

$$\dot{\epsilon}_{ij}^p = \frac{3}{2} \left[\frac{f'(\bar{\sigma})}{\bar{\sigma}} \right] s_{ij} d\bar{\sigma} \quad (3.1)$$

where $\bar{\sigma}^2 = 3J_2 = \frac{3}{2} s_{ij}^2$

and the uniaxial stress strain law has the form

$$\epsilon^p = f(\sigma)$$

so that $f'(\sigma) = \frac{df}{d\sigma}$

The function $f(\sigma)$ was obtained from the stress/strain relationship for the aluminum alloy given in Fig. 3.2. In this figure it should be noted that the stress reaches a limiting value of 155 MPa.

The general case, subjected to macro stress Σ_x , Σ_y , and Σ_{xy} , was analyzed using the element shown in Fig. 3.4. This covers the whole of the cyclically repeating cell. When the macro stress state is symmetric or anti-symmetric just a quarter of the repeating cell need to be analyzed (Fig. 3.5).

Following the homogenization procedure described in Section 2 the displacement field has the form

$$\begin{aligned} U(x,y) &= \bar{U}(x,y) + E_x \cdot x + E_{xy} \cdot y \\ V(x,y) &= \bar{V}(x,y) + E_y \cdot y + E_{xy} \cdot x \end{aligned}$$

where \bar{U}, \bar{V} is the periodic component. Taking nodes A and D with the same value of $x = a$ and nodes B and C with $y = b$. The boundary conditions imposed are;

$$\begin{aligned} U_D - U_A &= E_{xy} \cdot D \\ V_D - V_A &= E_{yy} \cdot D \\ U_C - U_B &= E_{xx} \cdot D \\ V_C - V_B &= E_{xy} \cdot D \end{aligned} \tag{3.2}$$

The values of E_{xx} , E_{yy} and E_{xy} are the loading inputs into the problem. The general case

was analyzed under two types of loading:

- (i) strain controlled loading, where loading was applied by proportionately increasing the macroscopic strains E_{xx} , E_{yy} , E_{xy} .
- (ii) stress controlled loading, when the loading was applied by proportionately increasing the resultant tractions F_x , F_y and F_{xy} that are related to the macro stress Σ_x , Σ_y and Σ_{xy} respectively.

3.2 The Elastic Calculation

The macro stress/strain relations in plane stress are written in the form:

$$\begin{aligned} E_{xx} &= \frac{\Sigma_{xx}}{M_{xx}} - \frac{\nu_{xy}}{M_{yy}} \cdot \Sigma_{yy} \\ E_{yy} &= \frac{\Sigma_{yy}}{M_{yy}} - \frac{\nu_{xy}}{M_{xx}} \cdot \Sigma_{xx} \\ \gamma_{xy} &= 2E_{xy} = \frac{\Sigma_{xy}}{G_{xy}} \end{aligned} \tag{3.3}$$

From finite element calculation in the elastic range the following values for the homogenized elastic constants were determined:

Elastic moduli $M_{xx} = 45700$ MPa
 $M_{yy} = 64900$ MPa
 $G_{xy} = 18700$ MPa

Poisson relation: $\nu_{xy} = 0.339$
 $\nu_{yx} = 0.239$

which satisfy the reciprocal relation

$$\frac{\nu_{xy}}{M_y} = \frac{\nu_{yx}}{M_x}$$

In matrix form the stress/strain relation in plane stress has the form

$$\begin{bmatrix} E_{xx} \\ E_{yy} \\ \gamma_{xy} \end{bmatrix} = 10^{-6} \begin{bmatrix} 21.9 & -5.2 & 0 \\ -5.2 & 15.4 & 0 \\ 0 & 0 & 53.5 \end{bmatrix} \begin{bmatrix} \Sigma_{xx} \\ \Sigma_{yy} \\ \Sigma_{xy} \end{bmatrix} \quad \left[\frac{1}{\text{Pa}} \right] \quad (3.4)$$

For comparison with the constants given in Eq. (3.3) the value of Young's Modulus and the aluminum alloy of the plate is 69.5 MPa. It can be seen that the presence of the slots substantially reduce the stiffness of the system for shear and transverse loading.

3.3 Elastic/Plastic Calculations

The general case was analyzed under two types of loading.

- (i) Strain controlled loading, where loading was applied by proportionally increasing the strains E_x , E_y and E_{xy} . This form of loading resulted in stable calculations and is especially useful for determining the Limit Load Surface which is more fully described later.
- (ii) Stress controlled loading, where the loading was applied by proportionally increasing the stress Σ_x , Σ_y and Σ_{xy} . This is the form of loading reported in the tests of Litewka and Sawczuk. Convergence was rather poor when the loads approached the limit load value.

Elastic/plastic calculations were performed for a uniaxial loading condition whose loading direction was defined by the angle α . This is the loading condition used by Litewka and Sawczuk. The calculations were repeated for different values of α which ranged between 0° and 90° . The computed macroscopic stress/strain results are shown in

Fig. 3.6 from which it may be seen that the experimental and calculated values are generally in good agreement. The predicted macroscopic stress/strain loading curves all show an initial elastic response, followed by an elastic/plastic region and a limit load condition for which the value of the load remains constant and further displacement is accommodated by plastic deformations. Since no failure criterion has been included in these calculations no failure is predicted from the calculations. In order to complete the relevant calculations a failure criterion must be included. In the absence of an obvious failure criterion this is not attempted at present, but shall be included later in an approximate analysis.

The limit condition is a surface which is a function of Σ_{xy} , Σ_{yy} and Σ_{xy} . The shape of this surface was obtained by performing elastic/plastic calculations for which the ratios of the strains remained constant. The calculations were repeated for various strain loading paths and the shape of the surfaces at the intersection with the section $\Sigma_{xy} = 0$, section $\Sigma_x = 0$ and section $\Sigma_y = 0$ are plotted in Figs. 3.7, 3.8 and 3.9 as are the strain rate vectors which satisfy the normality condition. The stress paths for different strain paths are shown in Fig. 3.7a and when the limit condition is reached the strain incremental vectors are normal to the surface.

An isometric plot of the 3D yield surface is given in Fig. 3.10. Only the $S_{xy} \geq 0$ region is shown since the plot will be symmetrical with respect to the $\Sigma_{xx}-\Sigma_{yy}$ plane.

It is interesting to observe the shape of the Limit Surface for the intersection with $\Sigma_{xy} = 0$. For this biaxial stress state the Limit Surface shown in Fig. 3.7 has the curious property that its shape is reminiscent of the Tresca yield condition in the first and third quadrants while the second and fourth quadrants indicate a condition more closely resembling the Mises condition. This topic is discussed more fully later.

4. A STUDY OF EDGE EFFECTS

In Section 2.3, it was illustrated how one of the errors introduced in the homogenization procedure is the imbalance of the applied macro stress Σ_{ij} and the calculated micro-stresses $\hat{\sigma}_{ij}$ along the component boundary. For elastic conditions it was determined that the total imbalance force over the length of the boundary of length d is two

orders smaller than the value of the macro stresses.

In order to study the influence of edge effects, an infinitely long strip in the x direction was analyzed. When the plate is subjected to axial stress Σ_{xx} (Fig. 3.11) the sections such as AA and BB remain straight during deformation and consequently, only the shaded portion shown in Fig. 3.7 needs to be analyzed.

The elastic solution for the case when $E_{xx} = 0.02\%$ and the elasto plastic solution for $E_{xx} = 1.5\%$ have been determined and the variation of stress σ_{yy} along the centerline is plotted as a function of the distance from the slot in Fig. 3.12.

If the slotted system were analyzed at the macro-level then one of the boundary conditions would be $\Sigma_{yy} = 0$. In fact while $\Sigma_{xx} = 0$ is satisfied on average the distribution of σ_{yy} at the micro-level is the same as that shown in Fig. 3.12. It can be observed that the error in the edge stresses is given by Eq. (2.2) and when applied to the current problem gives

$$\rho_{yy} = \sigma_{yy} - \Sigma_{yy}$$

It is noted that

$$\int_0^{D/2} \rho_{yy} dx = 0$$

because $\int_0^{D/2} \sigma_{yy} dx = 0$ (Fig. 3.12a).

Hence the stresses obtained from the homogenized solution are in equilibrium with the applied macro-stress, provided equilibrium over the cell length is considered. However equilibrium is not satisfied at every point of the boundary. From St. Venant principle it is to be expected that the homogenized solution is valid at a small distance from the edge. Reference to the solution of the strip problem indicate that the stresses and strains in the elements coincide everywhere with the homogenized solution with the exception of the edge elements. This observation is illustrated by Table 1 which gives the stress σ_{yy} at

different locations in the strip. It can be seen that the stresses are equal at the same location within the elements except for the edge elements, from which it can be deduced that the deviation from the homogenized solution is only one layer thick. This result is applicable for a continuous fiber reinforced composite loaded in the transverse direction but is not for loading in the longitudinal direction.

Table 1

Seven Cell Strip - $\alpha = 90$
 σ_{yy} Along Const Sections
 Elastic Solution - for $E_{xx} = 0.02\%$

x	y = 0.225	10.225	20.225	30.225
0.225	-0.13	-2.32	-2.32	-2.32
1.000	0.02	-2.15	-2.15	-2.15
1.775	-0.09	-1.96	-1.95	-1.95
2.225	-0.17	-1.45	-1.44	-1.44
3.000	-0.42	-0.25	-0.24	-0.24
3.775	0.30	2.19	2.19	2.19
4.056	0.45	3.28	3.28	3.28
4.250	0.31	3.65	3.64	3.64
4.444	0.15	3.92	3.91	3.91
4.556	0.42	4.35	4.34	4.34
4.750	0.60	4.66	4.65	4.65
4.944	0.39	4.64	4.63	4.63

The computations were extended to a loading level sufficiently high to cause extensive plastic deformations. The stress distribution σ_{yy} along the centerline are shown in Fig. 12b which are in equilibrium with the macrostress $\Sigma_{yy} = 0$. From the finite element calculations the observation can again be made that the stress distributions are the same for all elements except for those in the edge elements. This observation can be deduced from the results given in Table 2 which show the variation in the stress field σ_{yy} along the x direction for the same section in adjacent elements.

Table 2
 Seven Cell Strip - $\alpha = 90$
 σ_{yy} Along $y=\text{const}$ Sections
 Plastic Solution - $E_{xx} = 1.5\%$

x	y = 0.225	10.225	20.225	30.225
0.225	8.11	-66.70	-65.90	-65.90
1.000	4.36	-52.90	-52.40	-52.40
1.775	-12.30	-42.70	-42.80	-42.80
2.225	7.96	-29.30	-29.70	-29.70
3.000	15.10	8.07	7.21	7.21
3.775	-6.55	39.00	39.00	39.00
4.056	-0.68	64.20	64.40	64.40
4.250	-9.39	79.60	80.00	80.00
4.444	-11.30	87.90	88.40	88.40
4.556	-14.70	94.50	94.70	94.70
4.750	-2.00	94.50	94.50	94.50
4.944	3.15	94.70	94.70	94.70

5. COMPUTATIONAL RESULTS AND COMPARISON WITH EXPERIMENT

The predictions of the homogenization calculations are compared with the experimental investigation performed by Litewka and Sawczuk [1] in Table 3 with elastic properties defined by the relation (3.3)

Table 3

	M_x	M_y	G_{xy}	ν_{xy}	ν_{yx}
Experiments	41870	60780	19520	0.294	0.206
Calculated	45700	64900	18700	0.339	0.239

The relations between the predictions and measurement are generally within 10%.

The reciprocal relation

$$\frac{v_{xy}}{M_y} = \frac{v_{yx}}{M_x}$$

is satisfied for the calculated constants and is closely satisfied by the experimental data which give the result

$$\frac{v_{xy}}{v_{yx}} \cdot \frac{M_x}{M_y} = 0.983$$

The macroscopic stress/strain relationships when the material is subject to uniaxial loading is given in Fig. 3.6 for different slot angles. The predictions compare with the experimental data with almost perfect agreement for all angle orientations except for $\alpha = \pi/6$ when the difference in stress increases with strain from 0% to 10%. This may be due to early localization of the deformation for this orientation. The calculations are unable to predict the strains at which failure occurs. The large displacement analysis required to determine the failure strains has not been performed. Instead a simplified analysis of this problem has been completed and is described in the Appendix C

The results of the approximate finite strain calculations are given in Figs. 3.13 and 3.14 in which the stress and strain at failure are plotted for different slot angles α and strain hardening exponents. The results are normalized with respect to the failure stress and strain of an unperforated plate. The experimental failure stress values are also plotted in Fig. 3.13 and indicate generally good agreement with the predictions of the approximate analysis for low hardening exponents. The predictions of the failure strains in Fig. 3.14 indicate that when α is greater than 20° there is a sudden decrease in the strain to failure. This prediction is in keeping with the experimental observations (Fig. 3.6).

6. DESCRIPTION OF LIMIT SURFACE AND CONSTITUTIVE EQUATION

The isometric projection of the limit surface is shown in Fig. 3.10. The lower bound calculations performed in the Appendix define a limit surface defined by intersecting

surfaces with the form

$$a_{ijkl} \sum_{ij} \sum_{kl} = \sigma_n^2 \quad (i, j, k, l = x, y)$$

where a_{ijkl} are defined in Eqn (B2) and σ_y is the material limit stress. There are eleven such relationships which indicate the complexity of the shape of the limit surface. In an attempt to simplify the problem an approximate analysis is developed in the Appendix B from which a simplified form of limit surface is given by three relationships instead of eleven

$$\Omega(\sum_{xx}, \sum_{yy}, \sum_{xy}) = \sigma_n^2$$

where

$$3\left(\frac{\sum_{xx}}{\sigma_n}\right)^2 + 12\left(\frac{\sum_{xy}}{\sigma_n}\right)^2 \leq 1 \quad (6.1)$$

$$\left(\frac{10}{9}\right)^2 \left[\frac{\sum_{yy}^2}{\sigma_n^2} + 3\frac{\sum_{xy}^2}{\sigma_n^2} \right] \leq 1$$

$$4\frac{\sum_{xx}^2}{\sigma_n^2} + \left(\frac{10}{9}\right)^2 \frac{\sum_{yy}^2}{\sigma_n^2} - \frac{20}{9} \frac{\sum_x \sum_y}{\sigma_n^2} + 3\left(\frac{10}{4}\right)^2 \frac{\sum_{xy}^2}{\sigma_n^2} \leq 1$$

The homogenization calculations have been used to develop the limit surface, but the means to formulate a closed-form mathematical description of the surface is less apparent. It is easy to fit Hill's generalized yield surface but this description does not pick up the shape shown in Fig. 3.7 for example. The procedure adopted here was to develop expressions for the surface based on approximate models and to select the constants of the approximate analysis to fit the results obtained from the homogenization procedures.

It is also difficult to develop constitutive equations for the plate which are valid

current procedure is that computational experiments can be performed to determine the properties of the system. One such set of experiments consists of applying to the plate increments of strain such that the ratio

$$\frac{\Delta E_{xx}}{\Delta E_{yy}} = k$$

where k is a constant. The history of stress for some such strain paths is shown in Fig. (3.7). The initial response is elastic when the stress increments are dictated by the elastic constitutive equation of Eqn. (3.4). However as the applied stress approaches the limit surface the trajectory of the stress path is influenced increasingly by plasticity. The final location of the stress point on the limit surface is dictated by the normality rule when the vector of strain increments is normal to the limit surface. For some strain paths the stress state can change rapidly as the response of the material changes from purely elastic to purely plastic. This is particularly true of the paths 3 and 4 shown in Fig. 3.7. The simplest means of describing such behavior is to assume the component behaves in an elastic-perfectly plastic manner. With this assumption the stress paths would initially follow elastic response until the limit surface is reached when the normality rule would dictate the location of the stress state. Such an assumption gives stress histories which are close to those observed by calculation as indicated by the simple paths shown in Fig. 3.7. Then the simple constitutive relations are given by the sum of elastic deformation and plastic deformation

$$\dot{E}_{ij} = C_{ijkl} \dot{\Sigma}_{kl} + \dot{E}_{ij}^p$$

where the matrix C_{ijkl} is given in Table 3 and the plastic deformation rate satisfies

$$\dot{E}_{ij}^p = \dot{\lambda} \frac{\partial \phi}{\partial \Sigma_{ij}}$$

where Φ has the form of the limit surface defined by Eqn. (6.1).

CONCLUDING REMARKS

It has been demonstrated that the procedures of homogenization can be used efficiently to determine the macroscopic properties of composite systems from the constituent properties. To investigate the efficiency of the procedure, a difficult problem was selected which involves very high stress gradients more severe than would normally be found in practice. The macroscopic response is highly anisotropic which is highly representative of the anisotropic effects of damage. Furthermore, both elastic and plastic properties have been investigated so that the application to practical systems with inelastic deformation should be able to proceed without difficulty. The internal state of composites is extremely complicated which underlines the need to formulate macroscopic constitutive equations with a limited number of state variables which represent the internal state at the micro level.

As a next step it is intended to apply the method to determine the macroscopic properties of metal-matrix composites when subjected to the type of loadings to be considered in the design process. The computational predictions are to be compared to the results of an experimental program. From this investigation constitutive equations shall be determined and couched in a form suitable for finite element calculations. An effort will be directed towards selecting the microstructure to optimize the performance during operation and the manufacturing process.

ACKNOWLEDGEMENT

This work was supported by a grant from the NASA-Lewis Research Center.

APPENDIX A: APPROXIMATE ANALYSIS OF PLATE PROPERTIES

Some approximate analyses are performed to serve as a check on the validity of the homogenization procedures and to provide insight into the physical behavior of the plate.

Approximate analyses for the elastic limit load and failure strains are now performed. These approximate calculations serve as check on the effectiveness of the homogeneization calculations and can also help to provide physical insight into the component behavior.

6.1 Elastic Constants

The elastic constants determined from the homogenization calculation are given in Table 3 when the elastic constants of the homogeneous material of the plate are

$$E = 69550 \text{ MPa and } \nu = 0.337$$

Bounding estimates for E_x and E_y can be obtained using guessed equilibrium stress and compatible strain fields.

To obtain an upper bound on M_x a compatible strain field is assumed to be

$$\epsilon_x = E_x; \quad \epsilon_y = -\nu E_x$$

where E_x is the macrostrain. Energy balance then gives

$$\frac{1}{2} M_x \epsilon_x^2 = \frac{1}{V} \left[\frac{E}{2} \cdot \epsilon_x^2 (0.95V) \right]$$

From these calculations the following results are obtained

$$M_x = 0.95E \quad \text{and} \quad \nu_{xy} = 0.337$$

To obtain a lower bound on M_x the following stress field is assumed in the ligaments

between the slots

$$\sigma_x = 2\Sigma_x \quad ; \quad \sigma_y = 0$$

Again using complementary energy balance

$$\frac{1}{2} \cdot \frac{\Sigma_x^2}{M_x} = \frac{1}{v} \left[\frac{1}{2E} (2\Sigma_x)^2 \frac{v}{2} \right]$$

from which

$$M_x = 0.5E$$

Similar procedures applied in the y direction give for the assumed strain calculations yields

$$E_y = 0.95E$$

while the stress field calculation gives

$$E_y = 0.9E$$

Calculations have also been performed by assuming the slots do not interact and the energy increase in the body is given by the energy change for a slot in an infinite body.

For calculations in the x direction and assuming that the slots can be represented by slits the elastic internal energy per unit area of the plate is found to be

$$U = \frac{\Sigma_x^2}{2E} + \frac{\pi a^2 \Sigma_x^2}{2E} n = \frac{\Sigma_x^2}{2E_x}$$

where n is the number of cracks per unit area and the cracks are assumed to be non-interacting.

In the present problem $a = 2.5\text{mm}$ and $n = 1/100$ so that

$$E_x = \frac{E}{1 + \pi a^2 n} = 0.72E$$

The summary of results of experimental and computed and approximate results for elastic constants.

	<u>Lower Bound</u>	<u>Experiment</u>	<u>Hom</u>	<u>Non-Interacting Cracks</u>	<u>Upper Bound</u>
x direction	0.5E	0.602E	0.66E	0.72E	0.95E
y direction	0.9E	0.874E	0.933E	1.00E	0.95E

The predictions of the homogenization procedure agree to within 10% of the experimental observations. The non-interacting results are the most consistent of the approximate procedures which use extremely simple calculations.

APPENDIX B: LIMIT LOAD SURFACE

The isometric projection of the limit surface obtained from the homogenization calculations is shown in Fig. 3.10. In spite of the fact that the Mises yield condition is used it can be seen that the yield surface for the plate demonstrates features of both Tresca and Mises type criteria. In order to study the shape of the yield surface more fully approximate solutions are now developed.

Lower Bound Stress Analysis

An equilibrium stress field for the plate is illustrated in Fig. A.1. It can be deduced that there are nine microstress fields σ_{xx} , σ_{yy} , σ_{xy} given in terms of the macro stresses Σ_{xx} , Σ_{yy} and Σ_{xy} applied to the perimeter of the plate element. In terms of the macrostress Σ_x , Σ_y , Σ_{xy} the element perimeter stresses are given by

$$\Sigma_{xx} = 0.5 \sigma_x \quad \Sigma_{yy} = 0.9 \sigma_y \quad \Sigma_{xy} = 0.4\tau \quad (\text{B.1})$$

The value of σ_x , σ_y and τ for the nine stress fields are given in Table A.1 and when these are substituted in the yield condition $\sigma_{xx}^2 + \sigma_{yy}^2 - \sigma_{xx}\sigma_{yy} + 3\sigma_{xy}^2 = \sigma_y^2$ then the following yield criteria are established.

$$\text{Field 1)} \quad \sigma_y^2 + 3\tau^2 \leq \sigma_0^2$$

$$\text{Field 2)} \quad \sigma_y^2 + \frac{\sigma_y\tau}{2} + \tau^2 \leq \sigma_0^2$$

$$\text{Field 3)} \quad \sigma_x^2 + \sigma_y^2 - \sigma_x\sigma_y + (\sigma_x + \sigma_y)\frac{\tau}{2} + \tau^2 \leq \sigma_0^2$$

$$\text{Field 4)} \quad \sigma_x^2 \leq \sigma_0^2$$

$$\text{Field 5)} \quad \sigma_y^2 \leq \sigma_0^2 \quad (\text{B.2})$$

$$\text{Field 6)} \quad \sigma_x^2 + \frac{\sigma_x \tau}{2} + \tau^2 \leq \sigma_0^2$$

$$\text{Field 7)} \quad \sigma_x^2 + \sigma_y^2 - \sigma_x \sigma_y + 3\tau^2 \leq \sigma_0^2$$

$$\text{Field 8)} \quad \sigma_x^2 + 3\tau^2 \leq \sigma_0^2$$

$$\text{Field 9)} \quad \sigma_x^2 + \sigma_y^2 - \sigma_x \sigma_y \leq \sigma_0^2$$

Table A1

Field	σ_{xx}	σ_{yy}	σ_{xy}
1	0	σ_y	τ
2	$\tau/2$	$\sigma_y + \tau/2$	$\tau/2$
3	$\sigma_x + \tau/2$	$\sigma_y + \tau/2$	$\tau/2$
4	σ_x	0	0
5	0	σ_y	0
6	$\sigma_x + \tau/2$	$\tau/2$	$\tau/2$
7	σ_x	σ_y	τ
8	σ_x	0	τ
9	σ_x	σ_y	0

The inequalities given in Eqns. (B.2) define lower bounds of the limit surface. Sections of the limit surface and the results of the lower bound calculations are shown in Figs. A.2-A.3 and A.4. Also shown in the figures are the yield conditions for the undamaged system. As is to be expected the equilibrium stress fields give a lower bound on the yield surface. Generally, the bounds are good except in the Σ_{yy} , Σ_{xy} intersection where the difference between the lower bound and the homogenization results can be considerable.

Approximate Limit Surface Analysis

Another analysis is performed using engineering approximations but which give results agreeing more closely with the numerical results.

Referring to Fig. A.5 the plate element has been divided into three sections I, II and III which represents the critical regions where unconstrained plastic deformation can occur.

The element I is subjected to the stress state

$$\sigma_n = 2\Sigma_x \qquad \tau_{nt} = 2\Sigma_{xy}$$

With the assumption that the strain in the t direction is $\epsilon_t = 0$ gives the result

$$\sigma_t = \frac{\sigma_n}{2} = \Sigma_x$$

Using this stress state in the limit condition

$$\sigma_u^2 = \sigma_n^2 + \sigma_t^2 - \sigma_n \sigma_t + 3\tau_{nt}^2 = 3\Sigma_x^2 + 12\Sigma_{xy}^2$$

where σ_u is the ultimate stress of the material gives the condition

$$3\left(\frac{\Sigma_x}{\sigma_u}\right)^2 + 12\left(\frac{\Sigma_{xy}}{\sigma_u}\right)^2 = 1 \qquad (B.1)$$

The element II is subjected to the average stress state

$$\sigma_n = \Sigma_y \left(\frac{10}{9}\right) \qquad \sigma_{nt} = \Sigma_{xy} \left(\frac{10}{9}\right)$$

With the assumption that the stress $\sigma_t = 0$ the limit load criterion becomes

$$1 = \left(\frac{10}{9}\right)^2 \left[\frac{\Sigma_y^2}{\sigma_u^2} + 3 \frac{\Sigma_{xy}^2}{\sigma_u^2} \right] \quad (\text{B.2})$$

With a stress field on element III given by

$$\sigma_n = 2\Sigma_x \quad \sigma_t = \frac{10}{9}\Sigma_y \quad \sigma_{tn} = \frac{10}{4}\Sigma_{xy} \quad (\text{B.3})$$

Then the limit condition for this element is

$$\sigma_u^2 = \sigma_n^2 + \sigma_t^2 - \sigma_n \sigma_t + 3\sigma_{tn}^2$$

or

$$1 = 4 \left(\frac{\Sigma_x}{\sigma_n} \right)^2 + \left(\frac{10}{9} \right)^2 \left(\frac{\Sigma_y}{\sigma_n} \right)^2 - \frac{20}{9} \frac{\Sigma_x \Sigma_y}{\sigma_n^2} + 3 \left(\frac{10}{4} \right)^2 \left(\frac{\Sigma_{xy}}{\sigma_n} \right)^2 \quad (\text{B.4})$$

The estimated yield conditions (B.1)-(B.3) are plotted in Figs. A.2, A.3 and A.4 which also show the calculated limit conditions. The conditions (B.1) and (B.2) compare well with the calculated values. However the predictions of (B.3) are less good.

To improve condition (B.4) it is modified by adjusting the constants in (B.3) so that it fits closely the relationship determined from the homogenization calculations. The relationship (B.4) is modified to give

$$\frac{8}{3} \left(\frac{\Sigma_x}{\sigma_u} \right)^2 + \left(\frac{100}{81} \right) \left(\frac{\Sigma_y}{\sigma_u} \right)^2 - 1.2 \left(\frac{\Sigma_x}{\sigma_u} \right) \left(\frac{\Sigma_y}{\sigma_u} \right) + \frac{19}{4} \left(\frac{\Sigma_{xy}}{\sigma_u} \right)^2 = 1 \quad (\text{B.5})$$

A simplified description of the limit surface is then given by the surfaces

$$3 \left(\frac{\Sigma_x}{\sigma_u} \right)^2 + 12 \left(\frac{\Sigma_{xy}}{\sigma_u} \right)^2 = 1$$

$$\frac{100}{81} \left[\left(\frac{\Sigma_y}{\sigma_u} \right)^2 + 3 \left(\frac{\Sigma_{xy}}{\sigma_u} \right)^2 \right] = 1$$

$$\frac{8}{3} \left(\frac{\Sigma_x}{\sigma_u} \right)^2 + \left(\frac{100}{81} \right) \left(\frac{\Sigma_y}{\sigma_u} \right)^2 - 1.2 \left(\frac{\Sigma_x}{\sigma_u} \right) \left(\frac{\Sigma_y}{\sigma_u} \right) + \frac{19}{4} \left(\frac{\Sigma_{xy}}{\sigma_u} \right)^2 = 1 \quad (\text{B.6})$$

APPENDIX C: APPROXIMATE ANALYSIS OF FAILURE STRAINS

An approximate finite strain analysis is now performed when the perforated plate is subject to uniaxial stress for different slot orientations. The failure analyses are applied to the two characteristic ligaments which experiments indicate are the sources of failure. Referring to Fig. A.6 the ligament I is the ligament in line with adjacent slots while ligament II is the ligament between laterally adjacent slots.

The constitutive law used is

$$\sigma_e = K\epsilon_e^n$$

where σ_e is the effective stress, ϵ_e the effective strain and K and n are material constants. The strain components are defined by the relationship

$$\frac{\epsilon_{ij}}{\epsilon_e} = \frac{s_{ij}}{\sigma_e}$$

where s_{ij} is the stress deviator.

The classical stability analysis for an undamaged homogeneous material subjected to a uniaxial stress state predicts the failure strain at the load maximum to be

$$\epsilon^0 = n$$

and the nominal stress at load maximum is

$$\sigma^0 = Kn^n \exp(-n)$$

Reference to Fig. 3.6 indicates a failure strain of the undamaged material to be 1.5% so that n for the material in question is

$$n = 0.015$$

Analysis of Ligament I

The plate is subjected to the macro stress σ shown in Fig. A.6 with stresses in ligament I

$$\sigma_n = \frac{2A_0}{A} \sigma_t \frac{D}{D - \ell_y} \sin^2 \alpha \quad \tau_{nt} = \frac{2A_0}{A} \sigma_t \frac{D}{D - \ell_y} \sin \alpha \cos \alpha$$

where A_0 is the original cross sectional area and A is the current cross sectional area of the ligament.

Making the assumption that the strain in the t direction is zero i.e. $\epsilon_t = 0$ gives

$$\sigma_t = \frac{\sigma_n}{2}$$

With the given approximate stress state the effective stress σ_e is

$$\sigma_e = \sqrt{3} \sin \alpha \left[1 - \frac{3}{4} \sin^2 \alpha \right]^{1/2} \frac{A_0}{A} \sigma_t \frac{D}{D - \ell_y}$$

Assuming a deformation theory for the plastic strains the ratio for ϵ_n/ϵ_{nt} can be determined in terms of stress deviators so that

$$\frac{\epsilon_n}{\epsilon_{nt}} = \frac{s_n}{s_{nt}} = \frac{1}{3} \cdot \frac{2\sigma_n - \sigma_t}{\tau_{nt}} = \frac{1}{2} \cdot \frac{\sin \alpha}{\cos \alpha}$$

and the effective strain is then

$$\epsilon_e^2 = \frac{2}{3} \epsilon_{ij} \epsilon_{ij} = \frac{4}{3} (\epsilon_n^2 + \epsilon_{nt}^2)$$

and

$$\epsilon_e = \frac{2}{\sqrt{3}} (1 + 4 \cot^2 \alpha)^{1/2} \epsilon_n$$

From the definition of finite strain

$$\frac{A}{A_0} = \exp(-\epsilon_n)$$

so that the stress/normal ligament strain ϵ_n relationship becomes

$$\sigma_t = \frac{\left(\frac{2}{\sqrt{3}}\right)^n (1 + 4 \cot^2 \alpha)^{n/2}}{\sin \alpha \left[1 - \frac{3}{4} \sin^2 \alpha\right]^{1/2}} \cdot K \epsilon_n^n \exp(-\epsilon_n) \cdot \frac{D - \ell y}{D}$$

From this expression the strain at the load maximum following the classical analysis is

$$\epsilon_n = n.$$

The strain in the longitudinal direction in the band is

$$\epsilon_t^I = \epsilon_n \sin^2 \alpha + 2 \epsilon_{nt} \sin \alpha \cos \alpha$$

and recalling that

$$\epsilon_{nt} = 2 \frac{\cos \alpha}{\sin \alpha} \epsilon_n$$

yields the strain in the longitudinal direction as

$$\epsilon_t^I = \left[\sin^2 \alpha + 4 \cos^2 \alpha \right] \epsilon_n$$

Referring to Fig. A.6 the average strain is

$$\bar{\epsilon}_\ell = \frac{(\ell_x / \sin \alpha) \epsilon_\ell^I}{(D / \sin \alpha)} = \frac{\ell_x}{D} [\sin^2 \alpha + 4 \cos^2 \alpha] \epsilon_n$$

At load maximum $\epsilon_n = n$ so that

$$\frac{\bar{\epsilon}_\ell}{\epsilon_\ell^0} = \frac{\ell_x}{D} [\sin^2 \alpha + 4 \cos^2 \alpha]$$

is the average failure strain.

Analysis of Ligament II

A similar analysis for ligament follows along similar lines except that the stress σ_t is taken to be zero. Then

$$\sigma_n = \frac{A_0}{A} \sigma_\ell \cos^2 \alpha \cdot \frac{D}{D - \ell_x}$$

$$\tau_{nt} = \frac{A_0}{A} \sigma_\ell \sin \alpha \cos \alpha \cdot \frac{D}{D - \ell_x}$$

$$\sigma_t = 0$$

Hence the effective stress σ_e is

$$\sigma_e = \cos \alpha [3 - 2 \cos^2 \alpha]^{1/2} \frac{A_0 \sigma_\ell}{A} \frac{D}{D - \ell_x}$$

and the corresponding strains are

$$\frac{\epsilon_n}{\epsilon_{nt}} = \frac{2 \cos \alpha}{3 \sin \alpha}$$

$$\epsilon_c^2 = [1 + 3 \tan^2 \alpha] \epsilon_n^2$$

The stress $\sigma_\ell - \epsilon_n$ relationship is then given by

$$\sigma_\ell = \frac{[1 + 3 \tan^2 \alpha]^{n/2}}{\cos \alpha [3 - 2 \cos^2 \alpha]^{1/2}} \cdot K \epsilon_n^n \exp(-\epsilon_n) \frac{D - \ell_x}{D}$$

In the band the strain in the longitudinal direction is

$$\epsilon_\ell^{\text{II}} = [\sin^2 \alpha + 4 \cos^2 \alpha] \epsilon_n$$

and the average strain in the longitudinal direction is

$$\bar{\epsilon}_\ell = \frac{(\ell y / \sin \alpha) \epsilon_\ell^{\text{II}}}{(D / \sin \alpha)} = \frac{\ell y}{D} [\sin^2 \alpha + 4 \cos^2 \alpha] \epsilon_n$$

At the load maximum $\epsilon_n = n$ which gives

$$\bar{\epsilon}_\ell = \frac{\ell y}{D} [\sin^2 \alpha + 4 \cos^2 \alpha] n$$

and

$$\frac{\bar{\epsilon}_\ell}{\epsilon_\ell^0} = \frac{\ell y}{D} [\sin^2 \alpha + 4 \cos^2 \alpha]$$

References

1. Léne, F., *Engineering Fracture Mechanics*, 25, 713-728, 1986.
2. Duvant, G., *Theoretical and Applied Mechanics*, (ed. W. Koiter), 119-132, North Holland, Amsterdam, 1979.
3. Litewka, A. and Sawczuk, A., "Experimental Evaluation of the Overall Anisotropic Material Response on Continuous Damage," *Mechanics of Material Behavior-Daniel C. Drucker Anniversary Volume* (G.J. Dvorak and R.T. Sheld, editors), Elsevier, Amsterdam, 1984, pp. 239-252.
4. Litewka, A. and Morzynska, A., "Theoretical and Experimental Study of Fracture for a Damaged Solid," *Res. Mechanica*, *27*, pp. 259-272, 1989.
5. ABAQUS

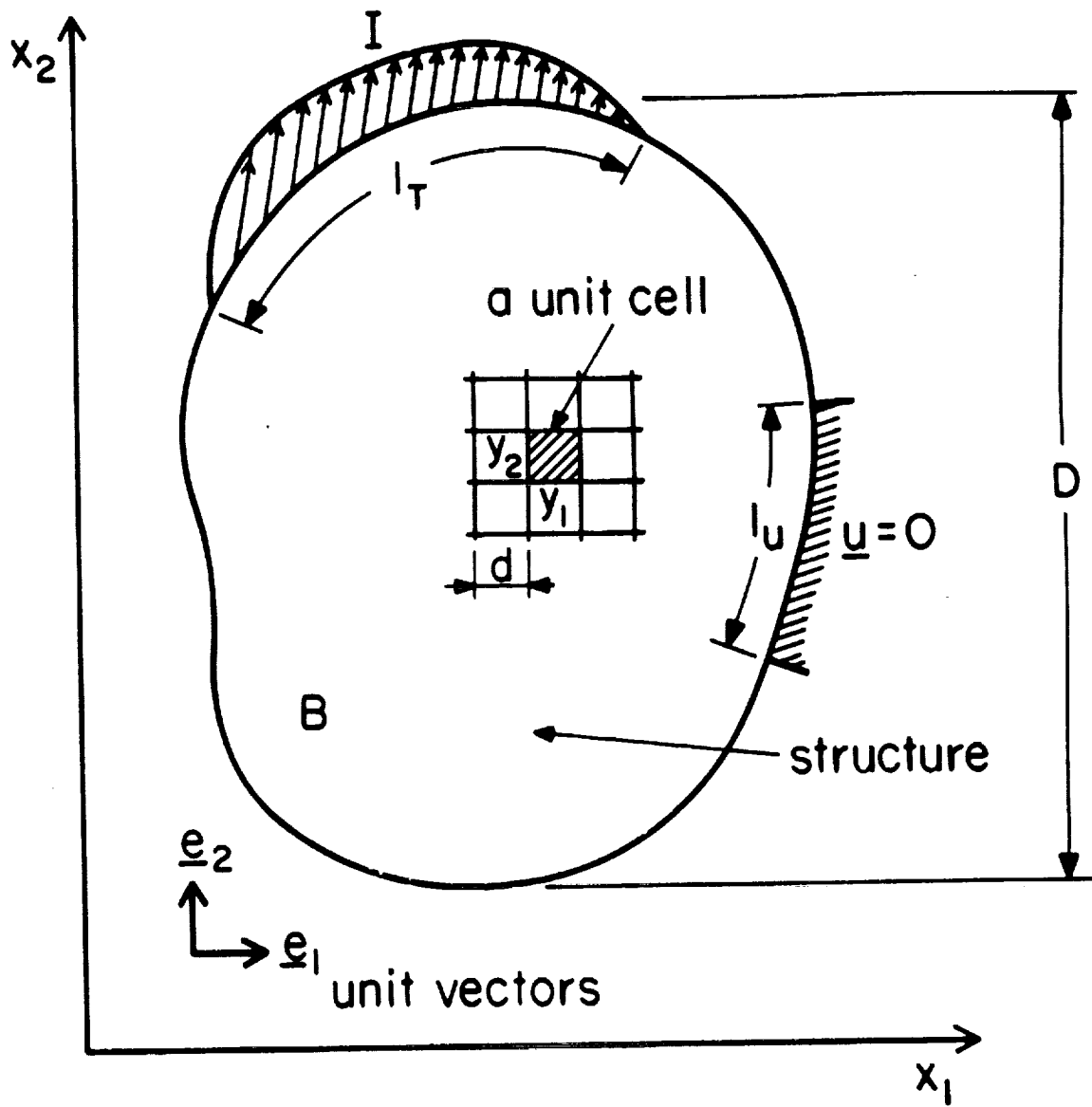


Fig. 2.1 A structure made of a periodic composite material.

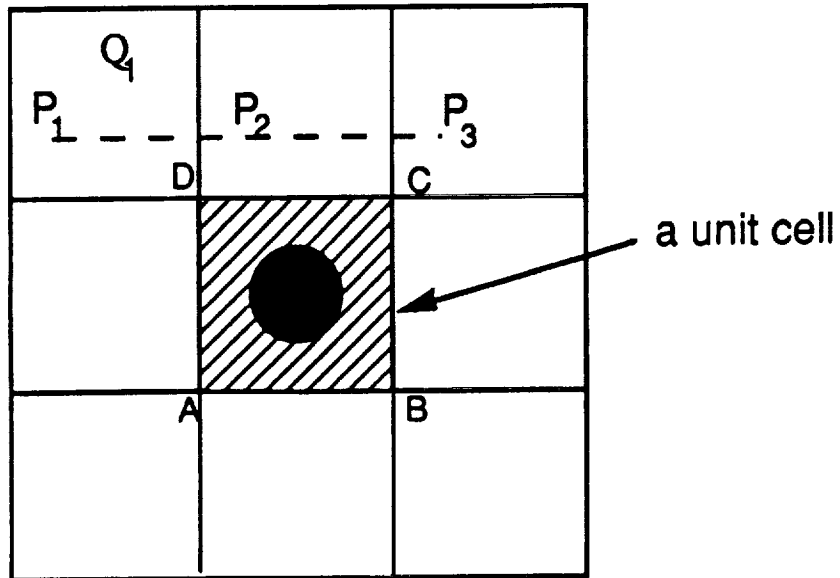


Fig. 2.2a A nine-cell sub-domain within the body shown in Fig. 2.1
 $P_1, P_2 \dots$: homologous points. ABCD: unit cell.

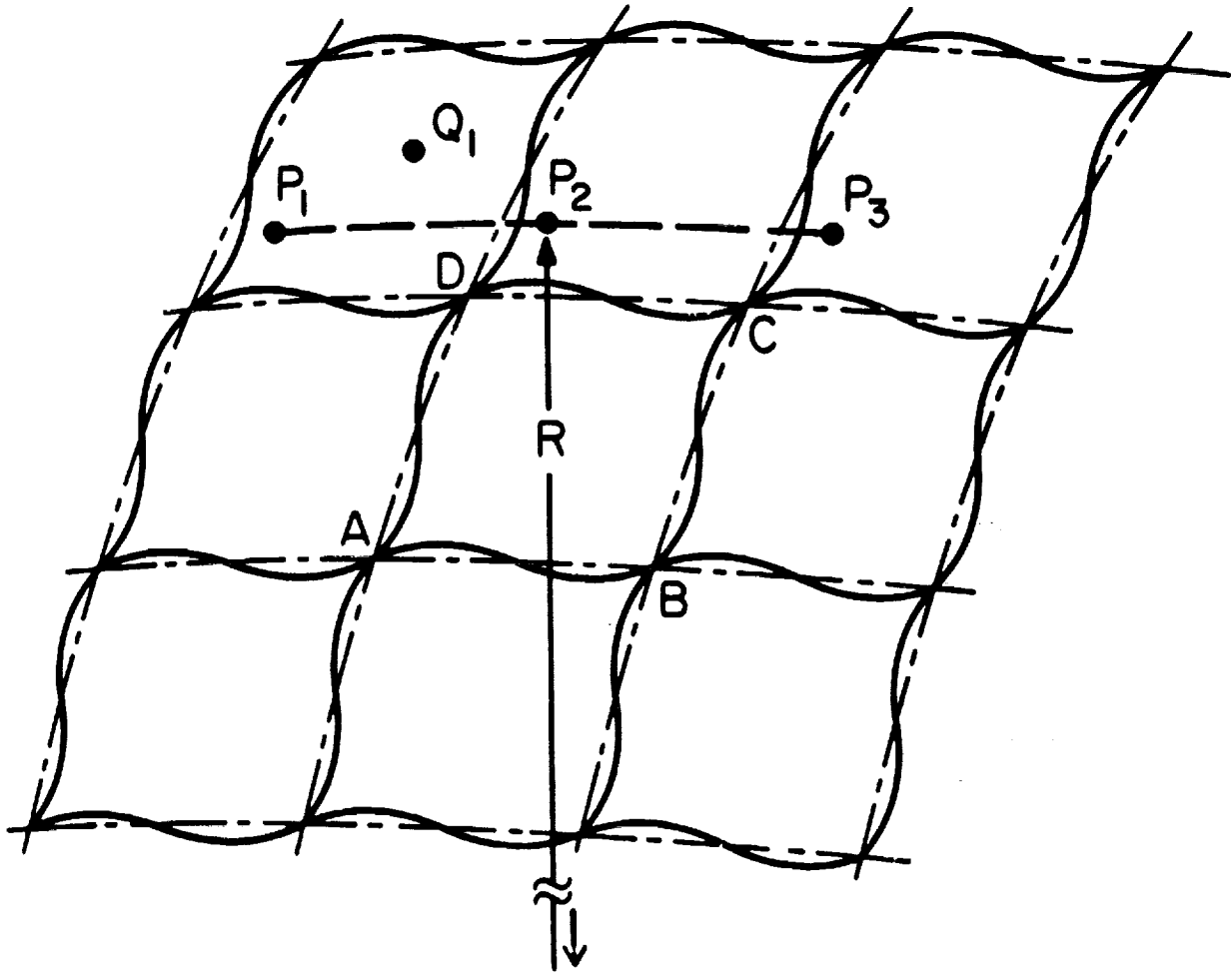


Fig. 2.2b Deformed shape of nine-cell sub-domain;

$\frac{R}{d} \gg 1$, R radius of circle passing through three consecutive homologous points.

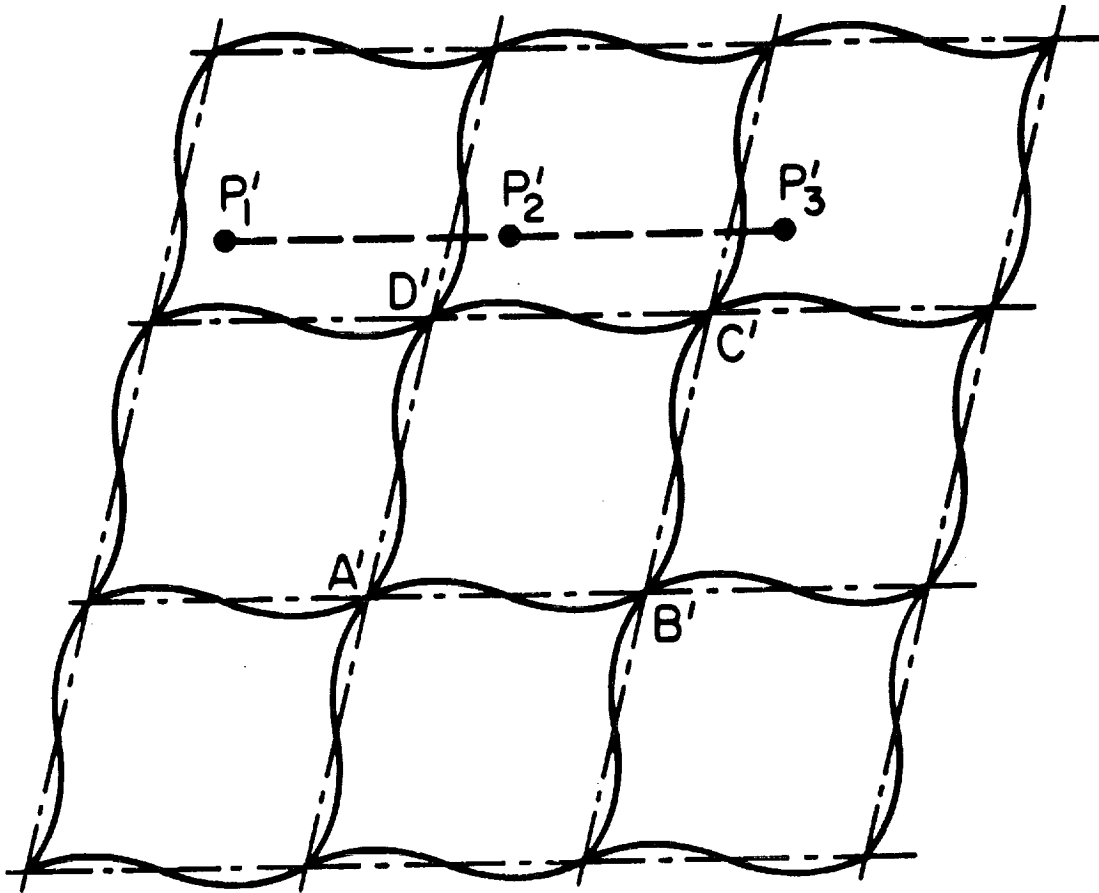


Fig. 2.2c Macroscopically homogenous deformation of nine-cell sub-domain is a good approximation to the deformed shape of Fig. 2.2b.

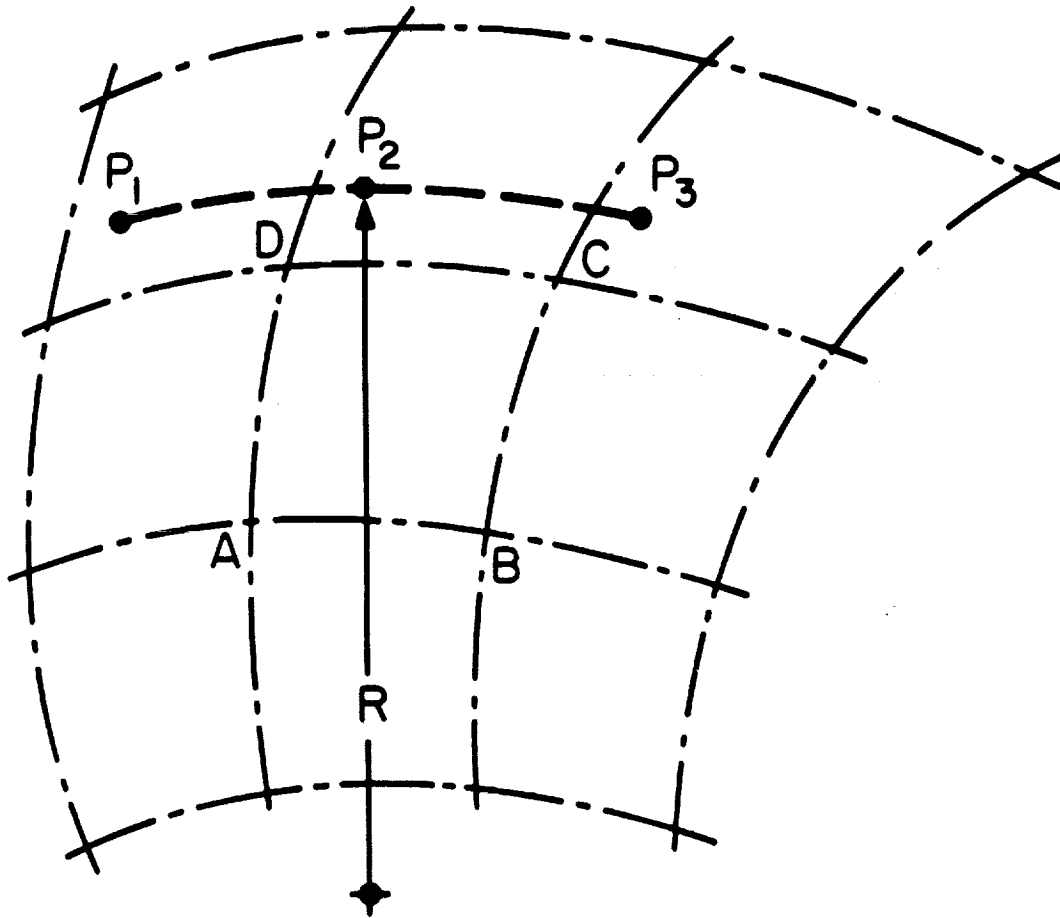


Fig. 2.2d The program of homogenization fails locally if the deformed shape sub-domain of the homogenized body is such that R is comparable to d . Such a situation can develop near a crack tip or when localized deformation occurs.

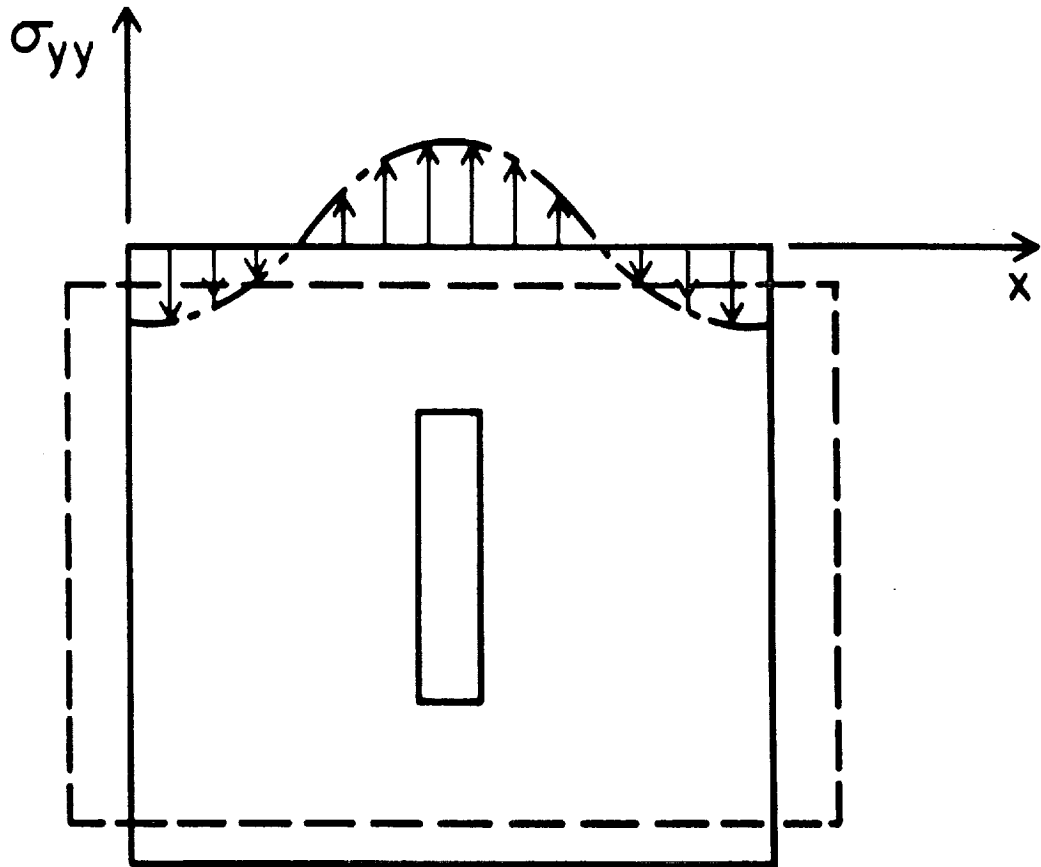


Fig. 2.2e Traction free boundaries vs/homogenization.

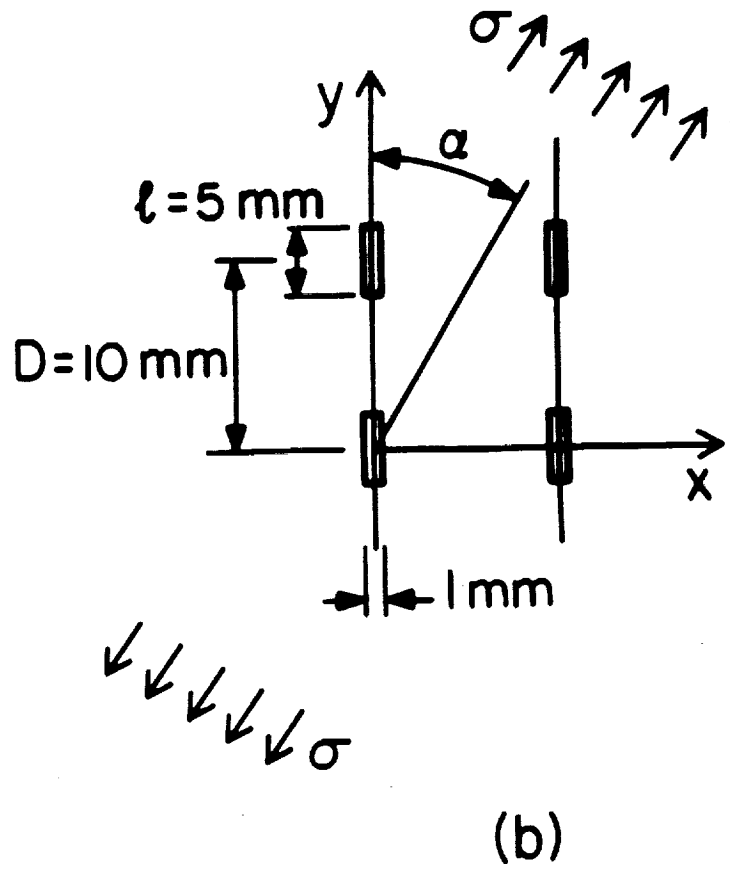
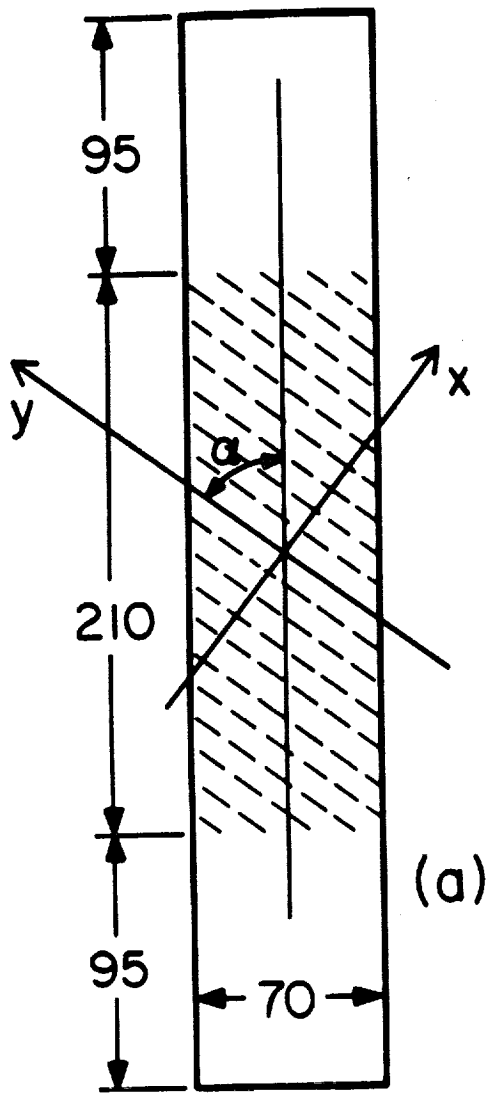


Fig. 3.1 a) Specimen with simulated damage.
 b) Dimensions of cracks.

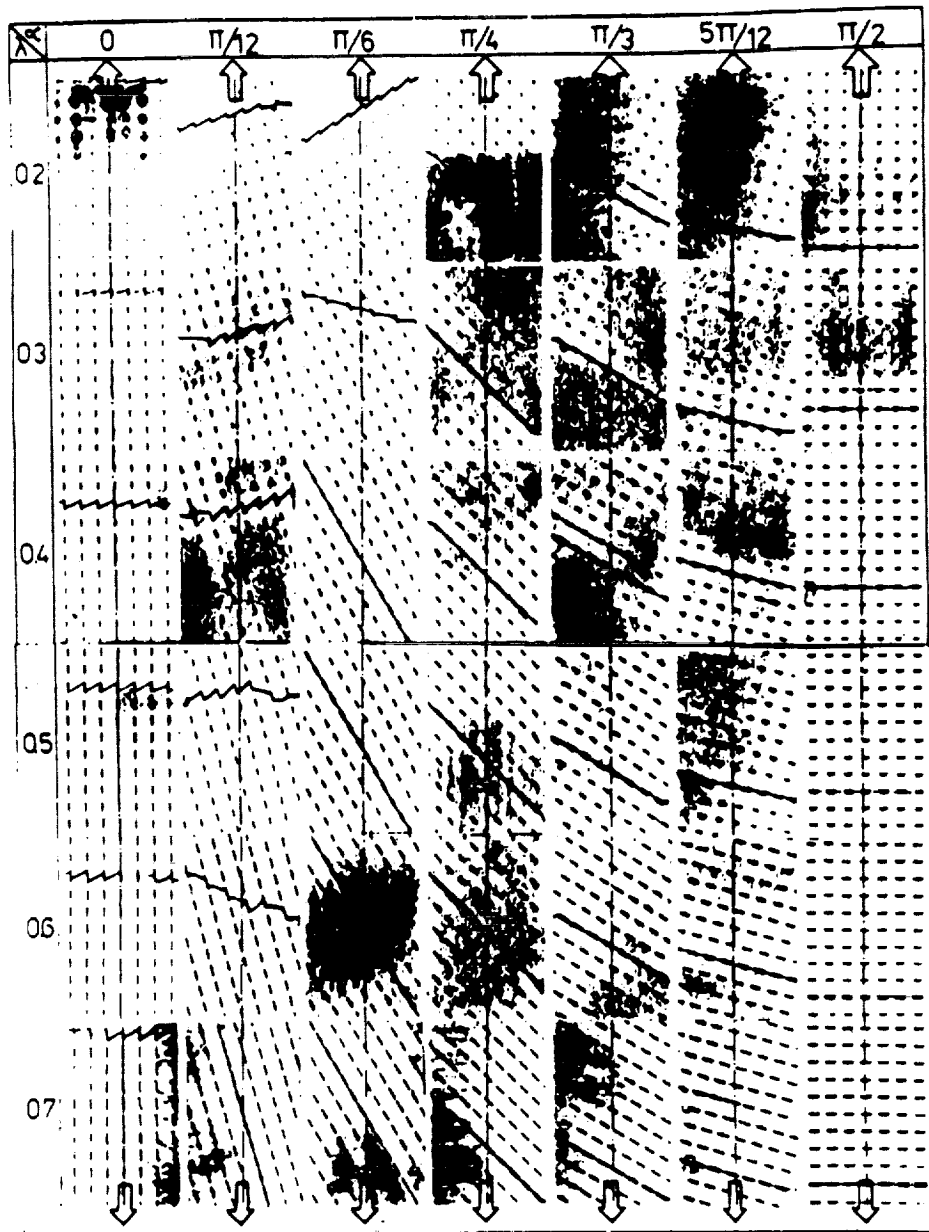


Fig. 3.3 Strain localization at failure.

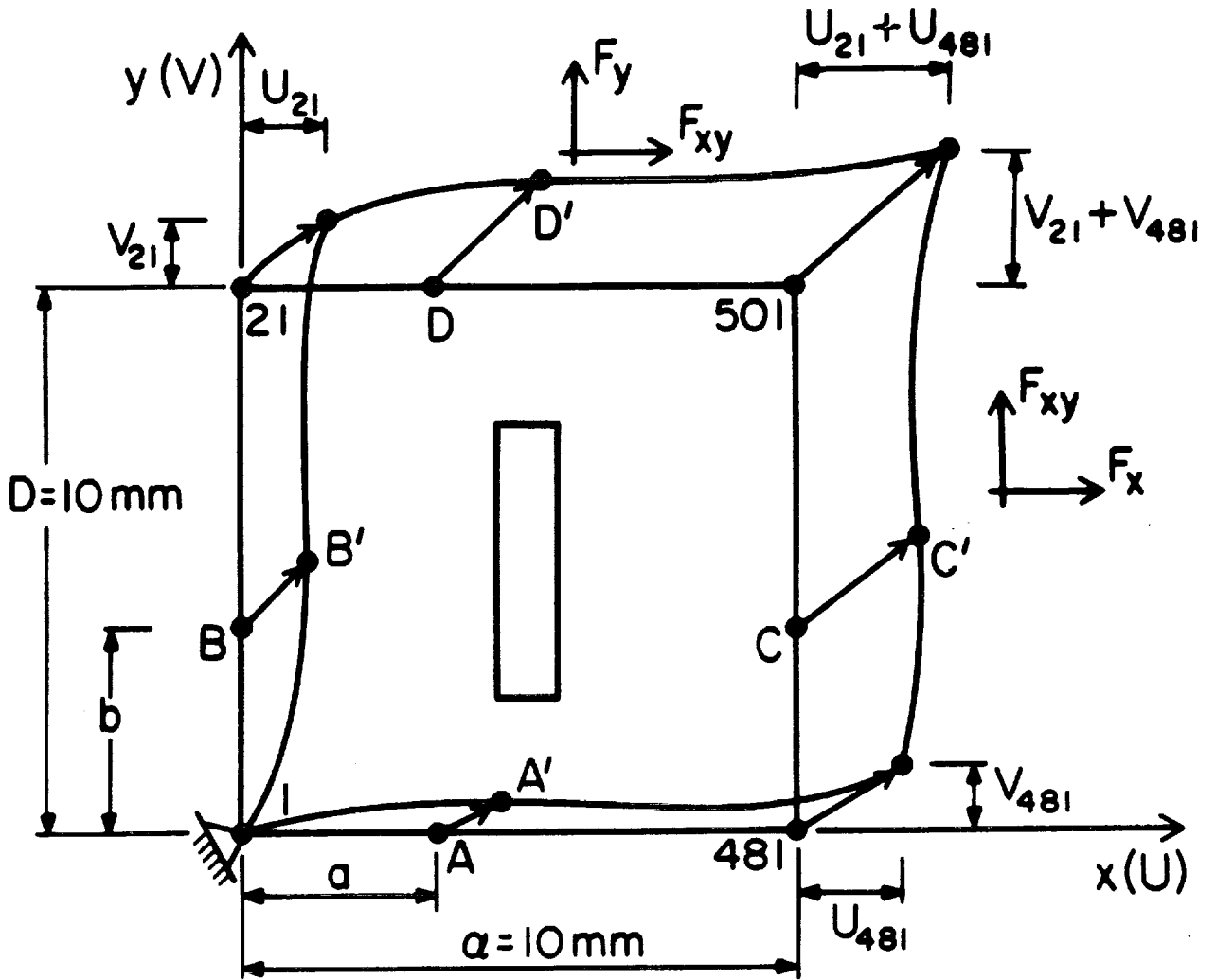


Fig. 3.4 Element used in homogenization process.

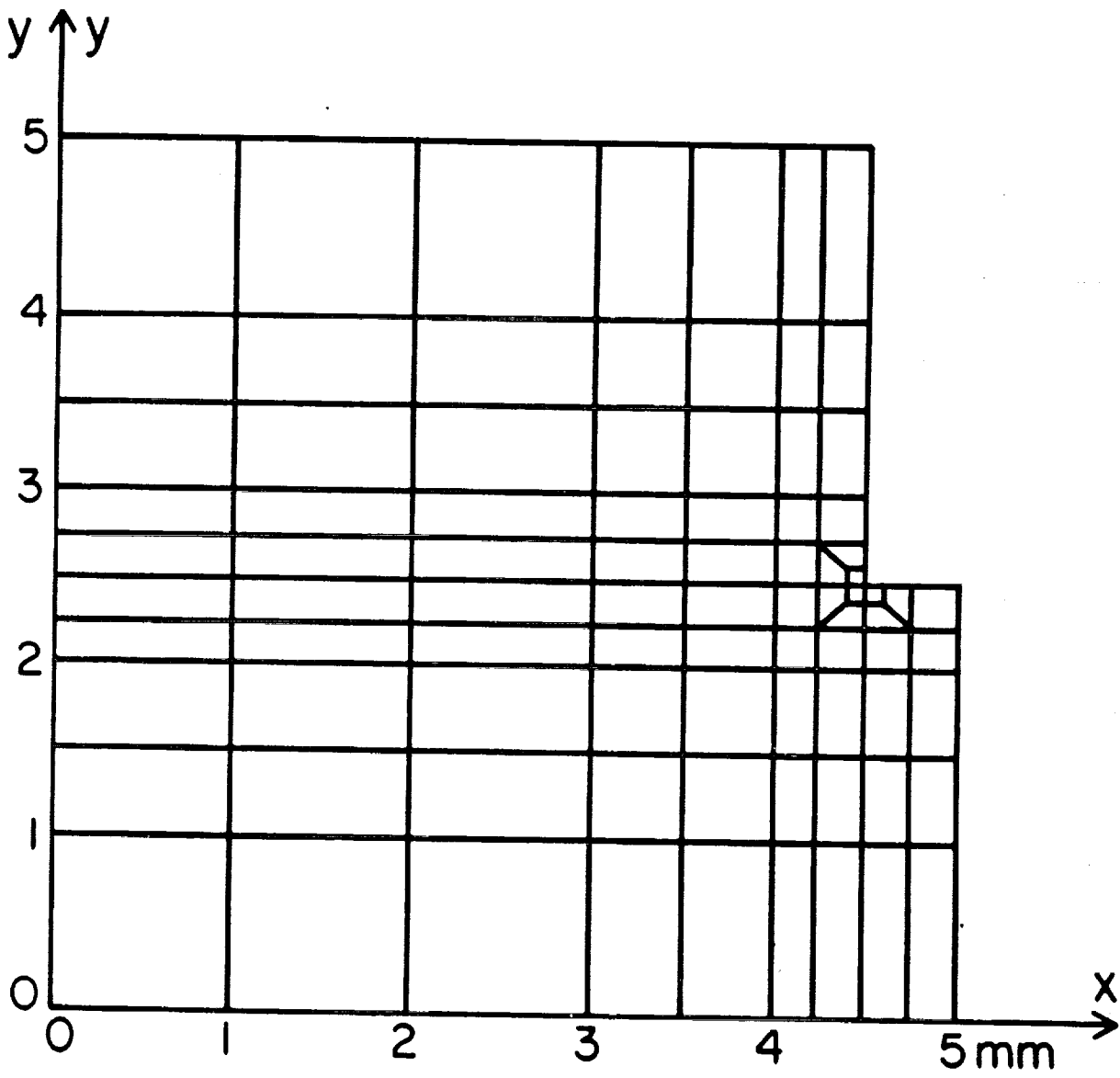


Fig. 3.5 Finite element representation used in homogenization process.

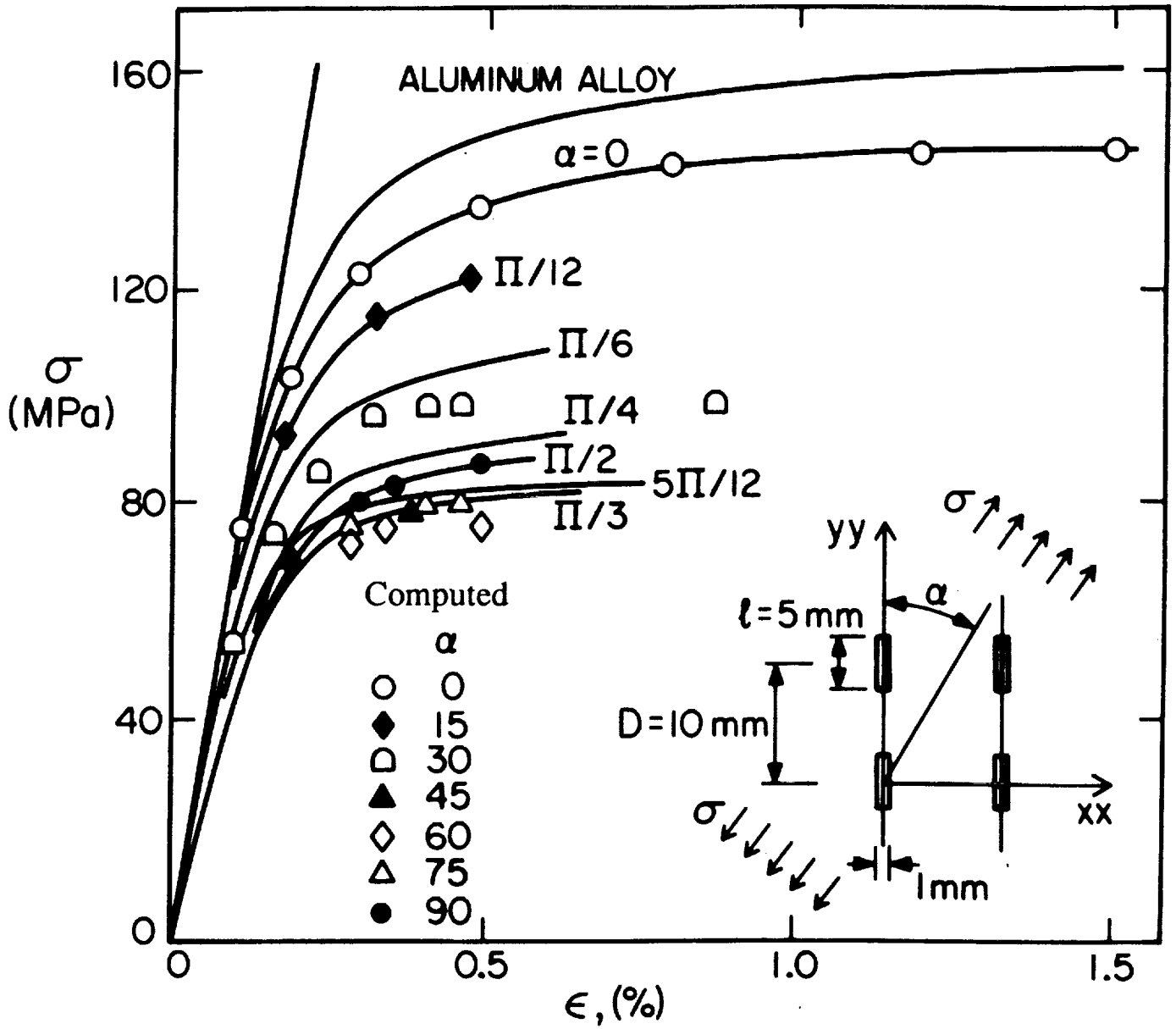


Fig. 3.6 Comparison of computed and experimental results.

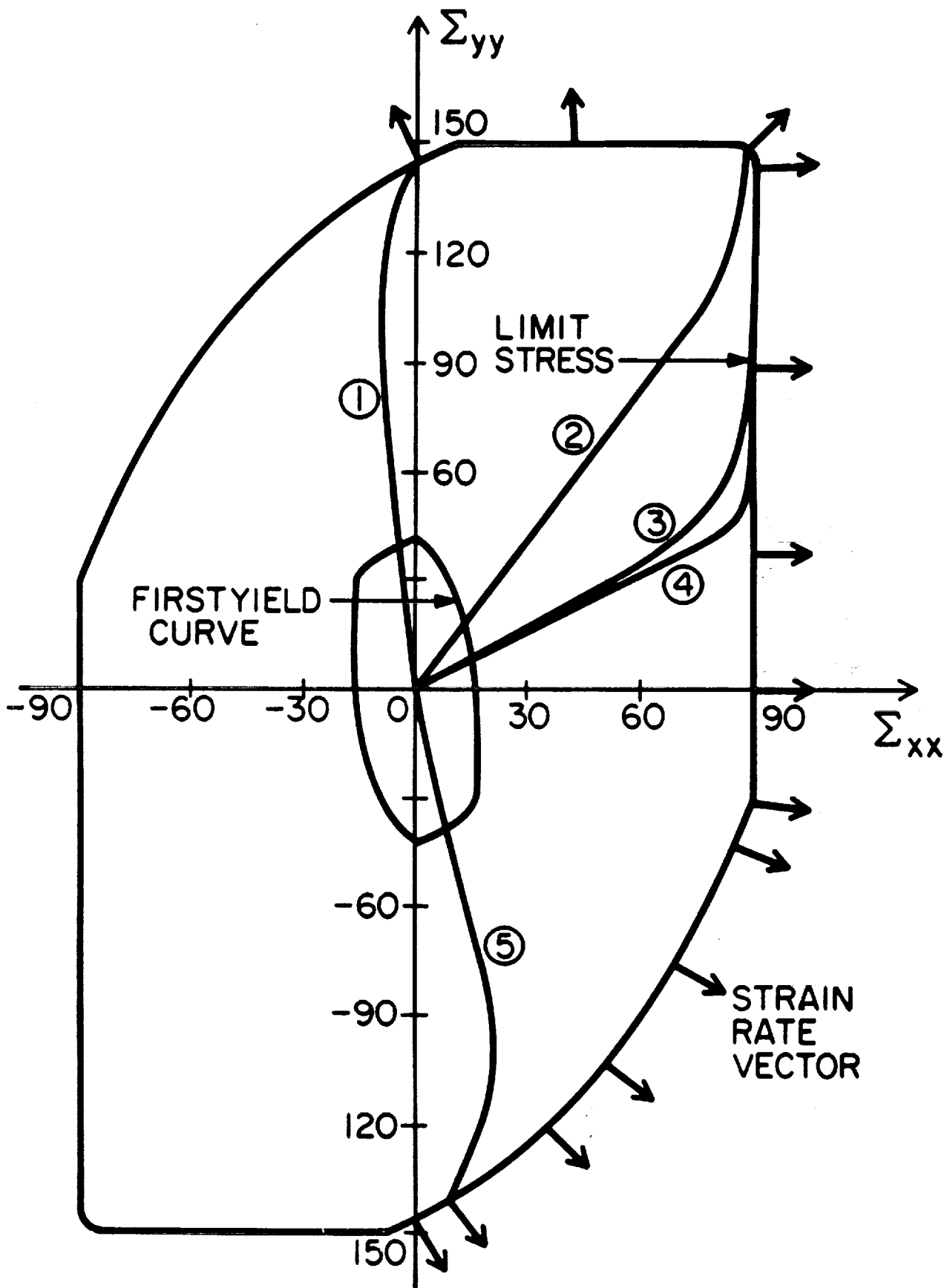


Fig. 3.7 Limit Surface in Σ_{xx} , Σ_{yy} plane.

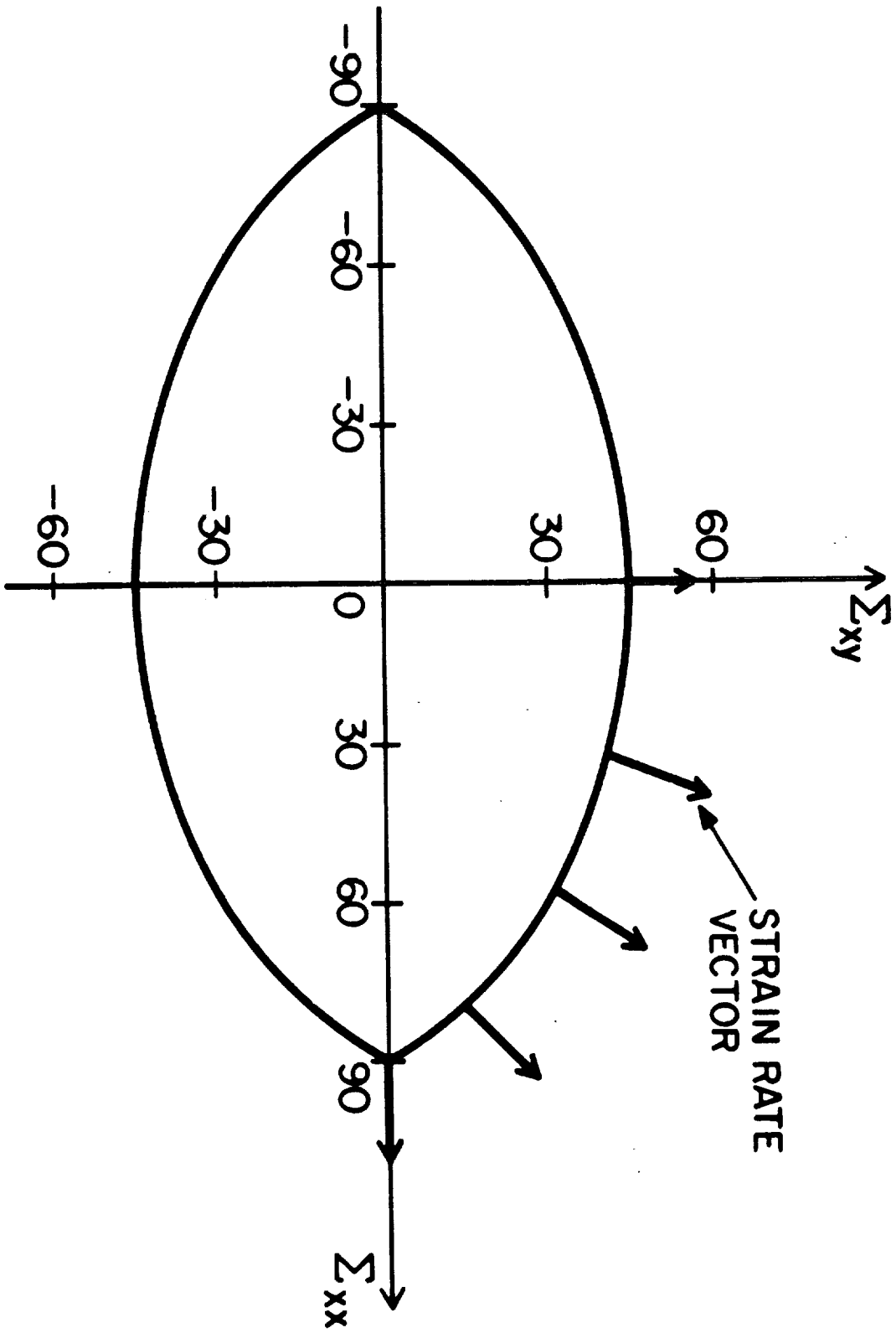


Fig. 3.8 Limit Surface in Σ_{xx} , Σ_{xy} plane.

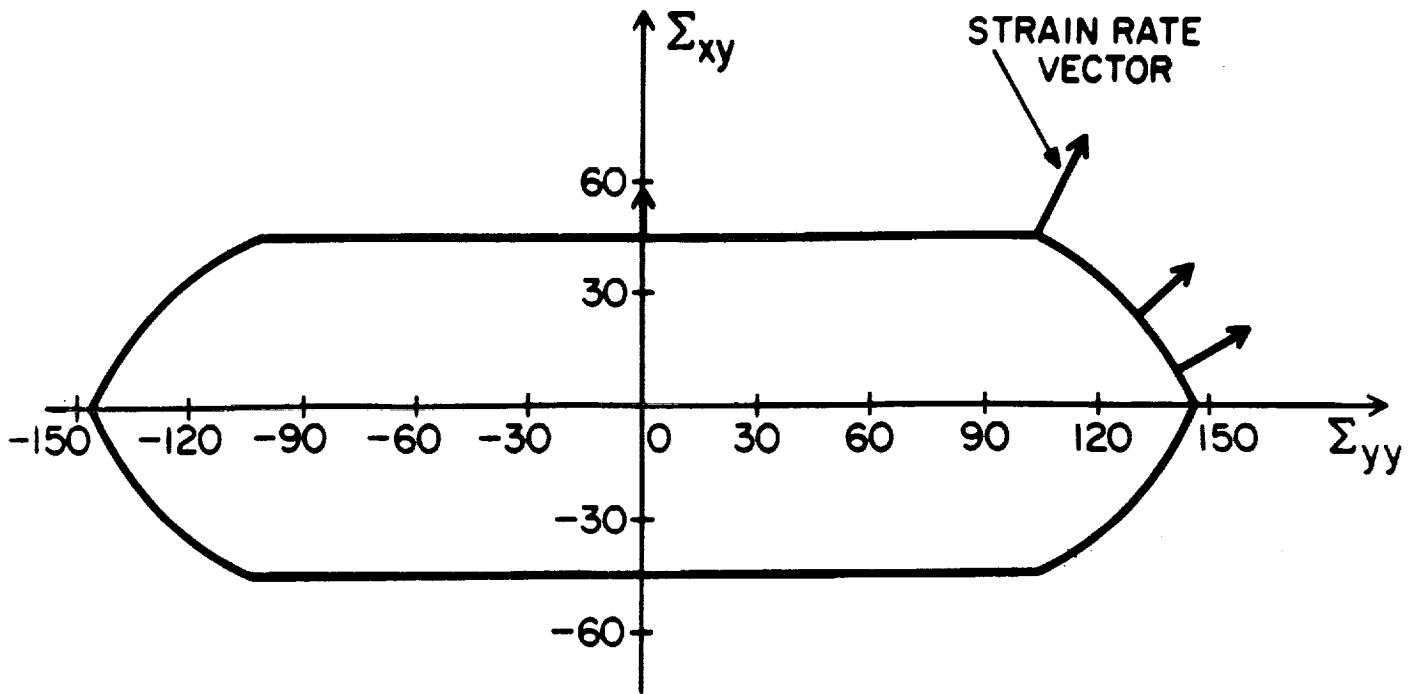


Fig. 3.9 Limit Surface in Σ_{yy} , Σ_{xy} plane.

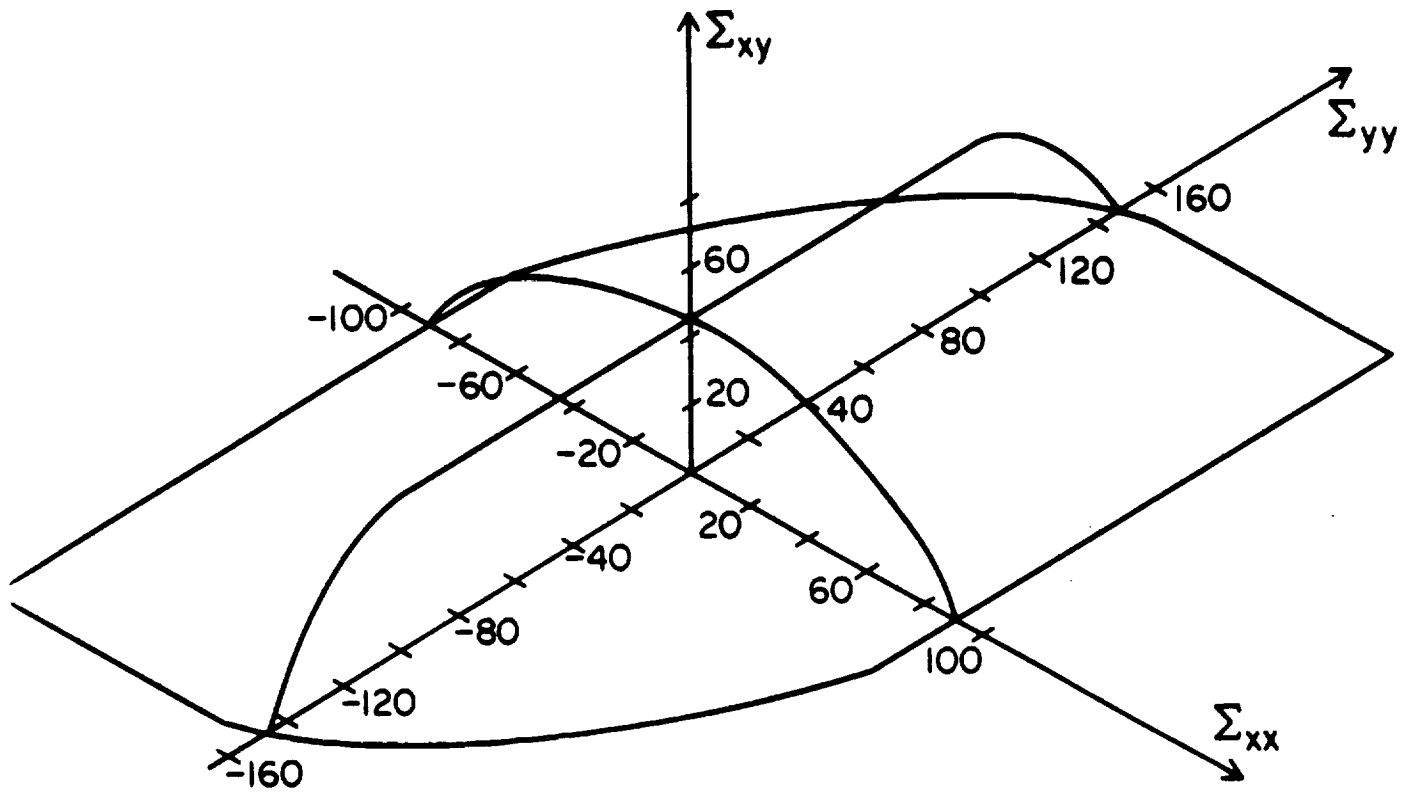


Fig. 3.10 Isometric view of limit surface.

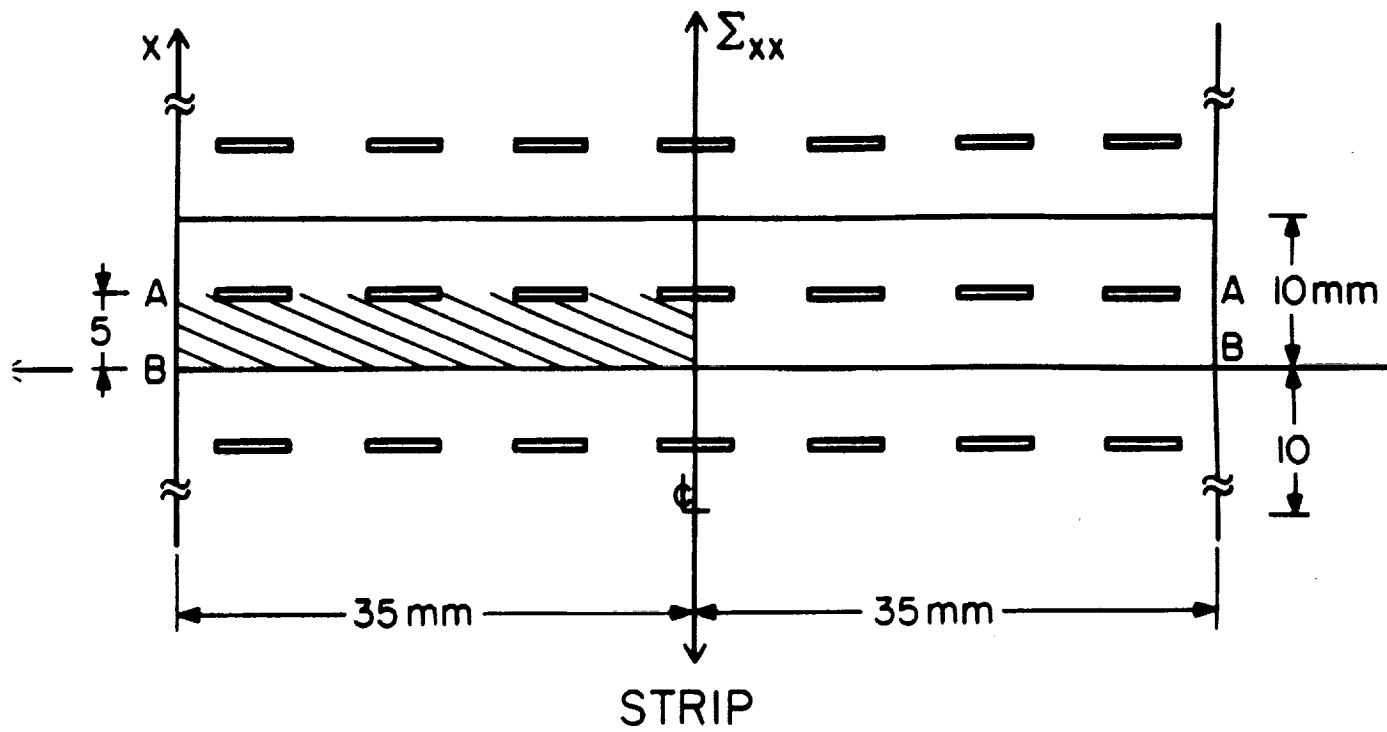


Fig. 3.11 Element used for edge effects.

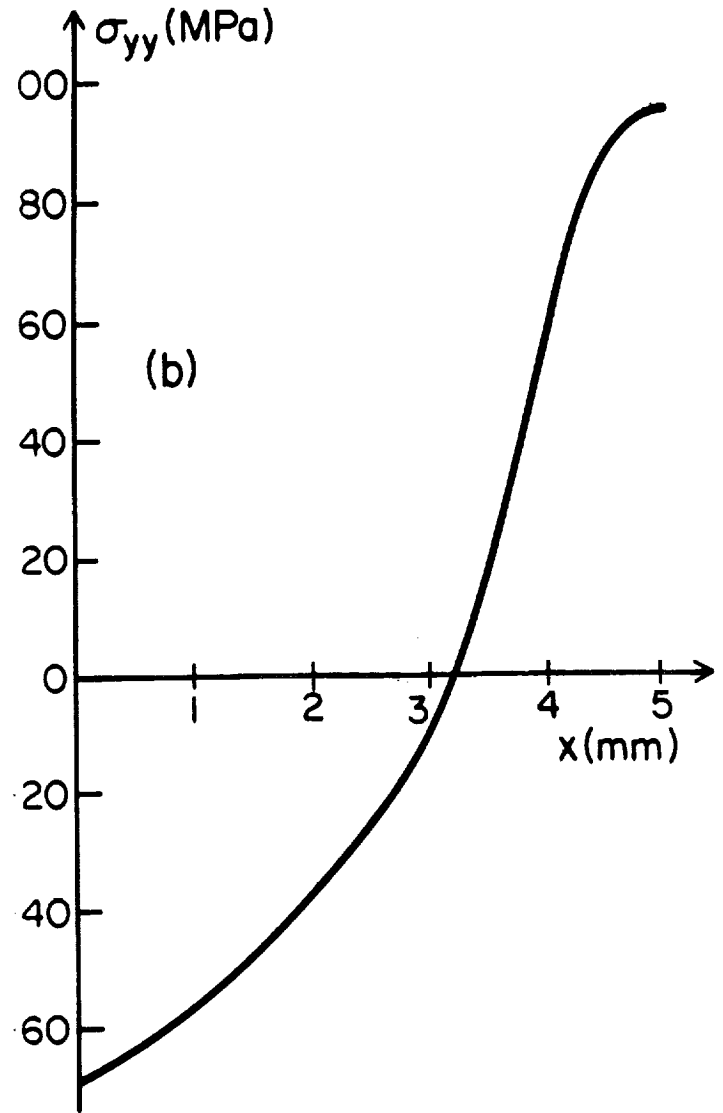
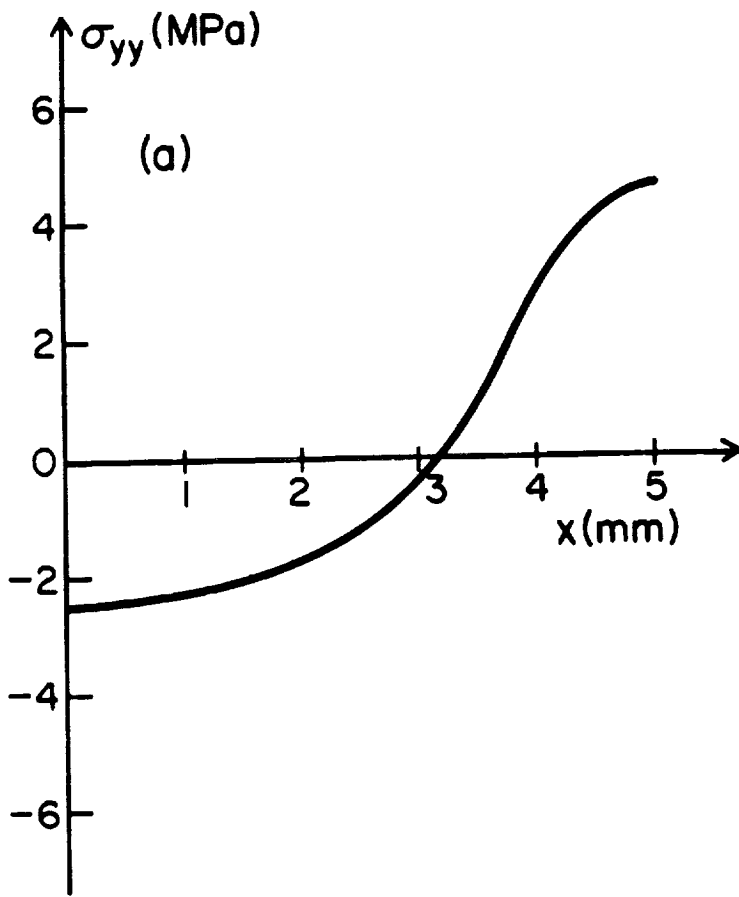


Fig. 3.12 Edge stress from homogenization calculations.

a) $E_{xx} = 0.2 \%$

b) $E_{xx} = 1.5 \%$

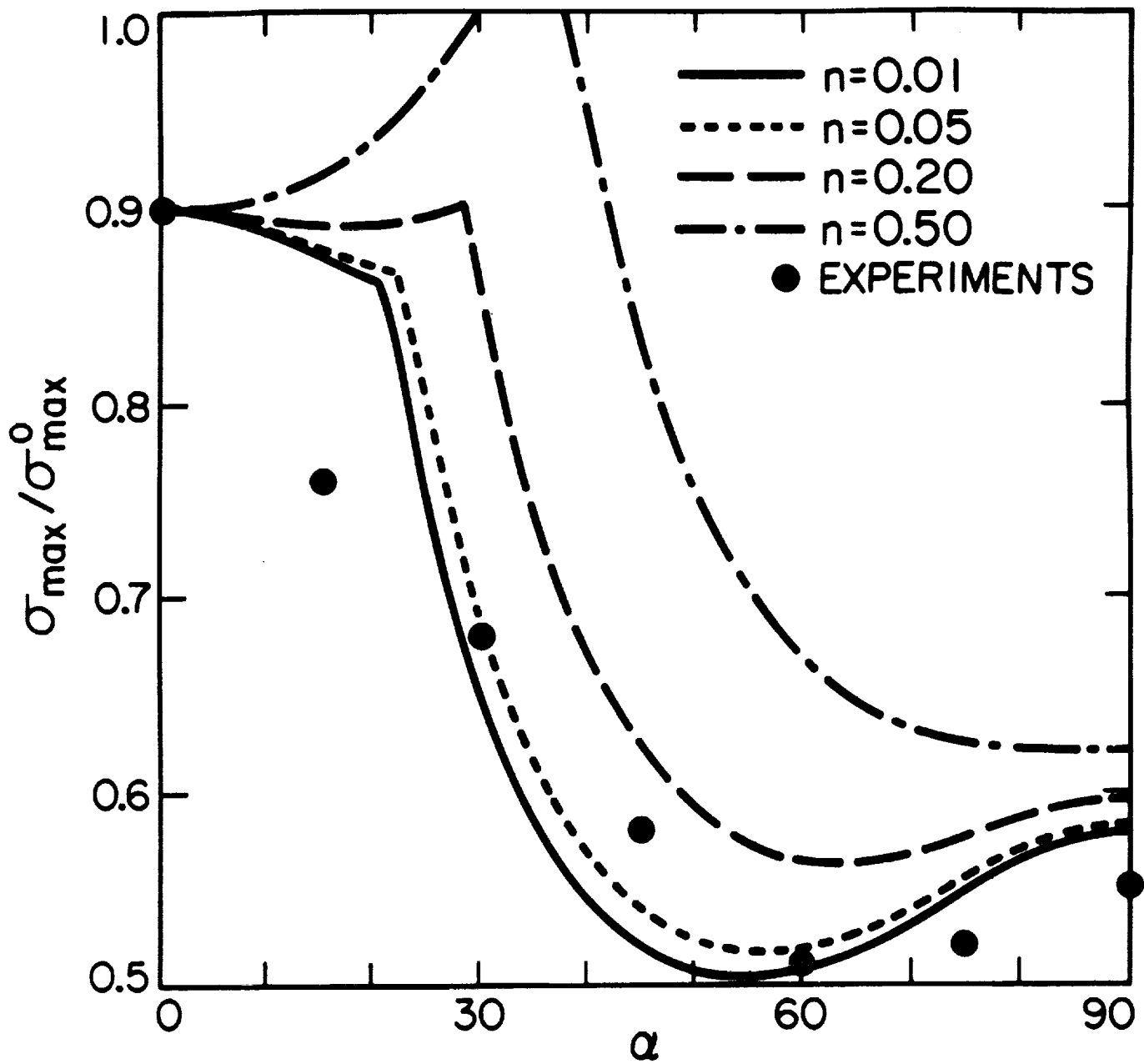


Fig. 3.13 Failure stress variation with damage angles.

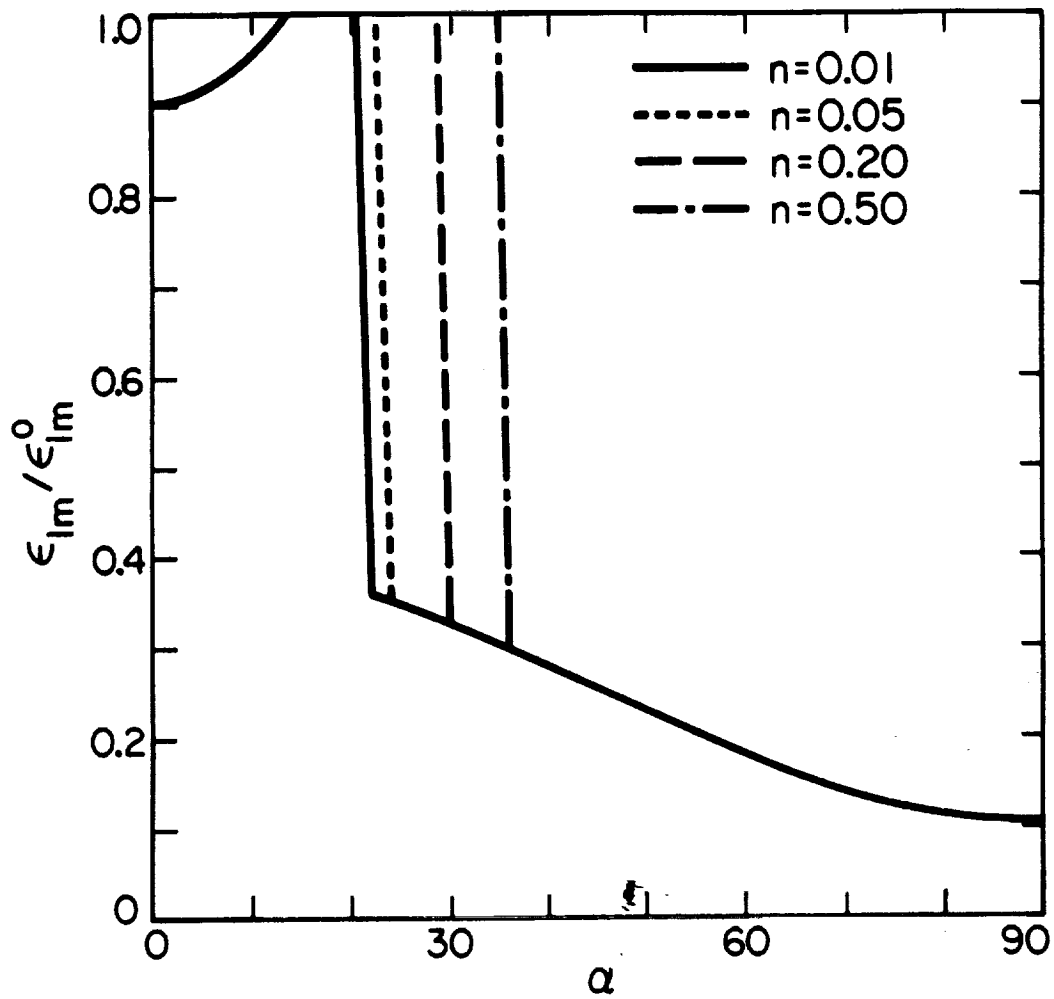


Fig. 3.14 Failure strain variation with damage angles.

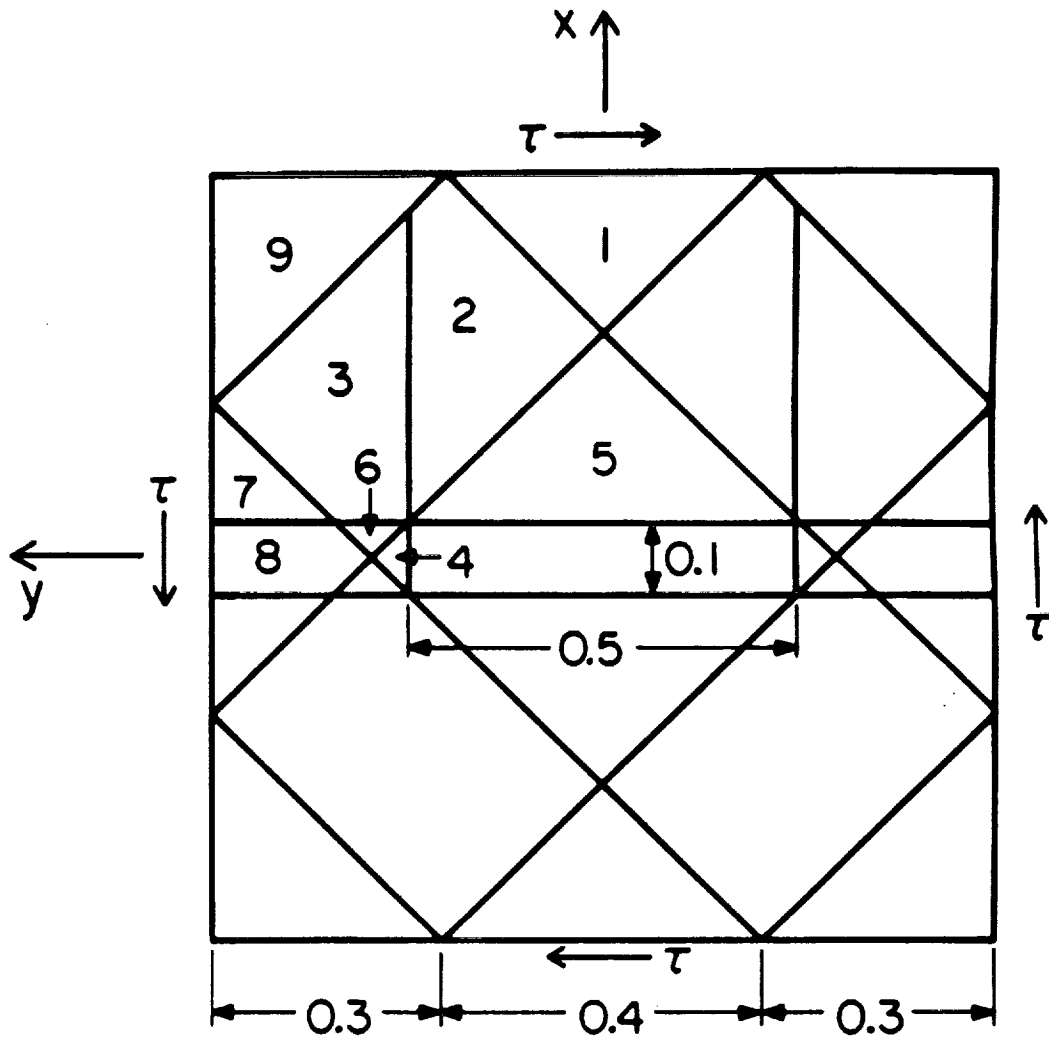


Fig. A.1 Equilibrium stress fields in element.

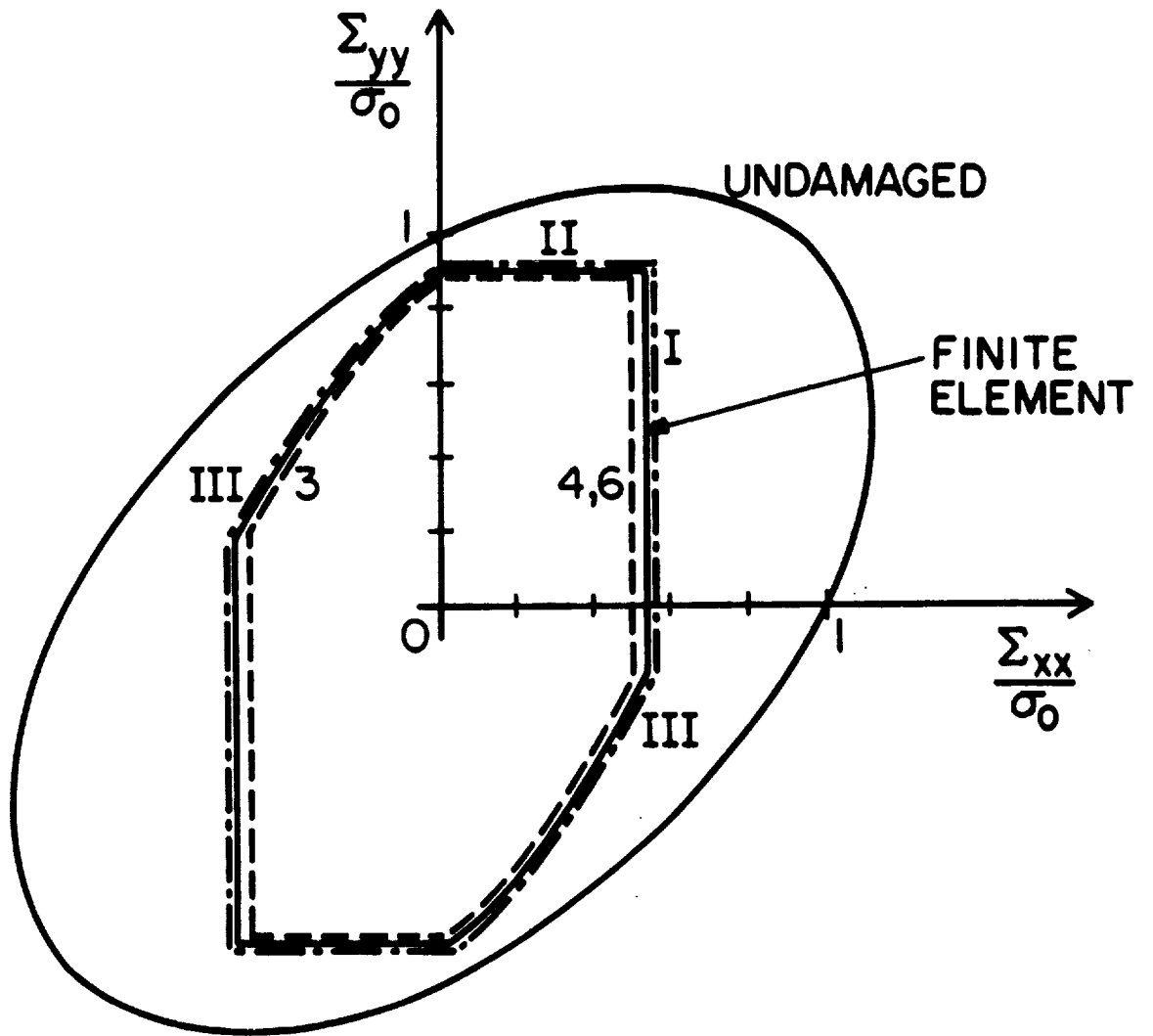


Fig. A.2 Comparison of Calculation and Approximate Limit Surface in Σ_{xx} , Σ_{yy} plane.

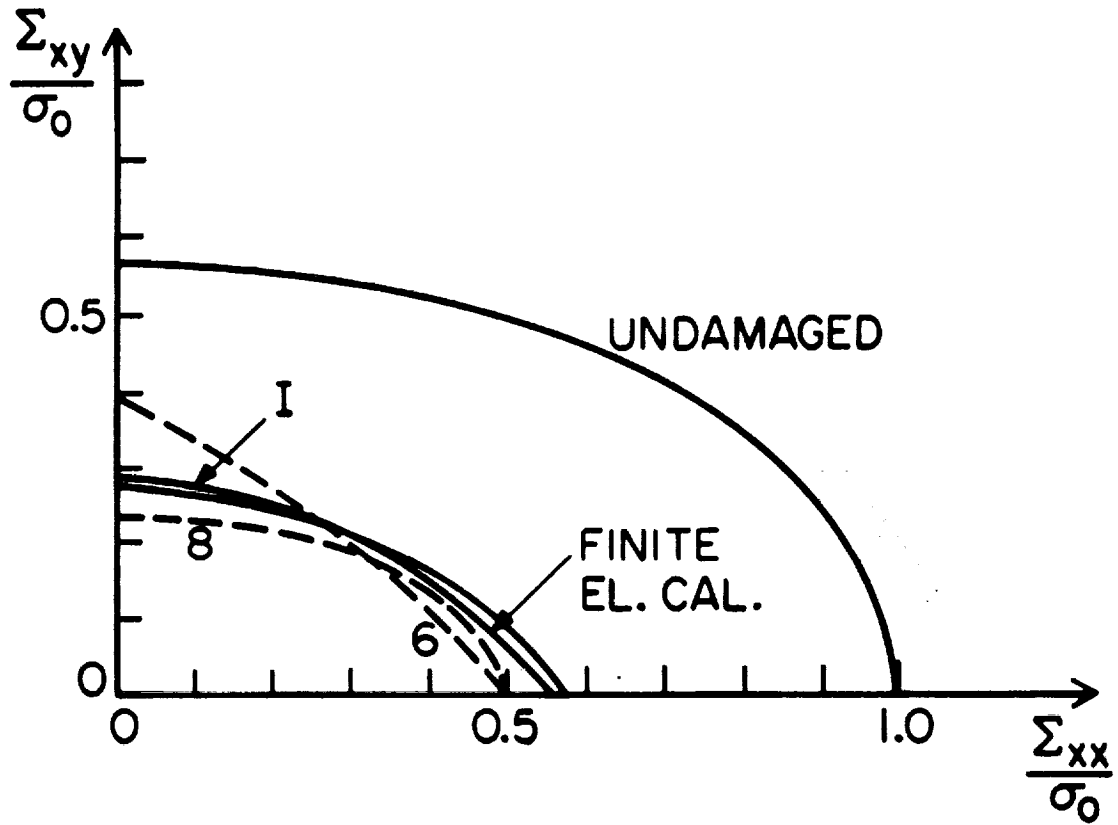


Fig. A.3 Comparison of Calculation and Approximate Limit Surface
in Σ_{xx} , Σ_{xy} plane.

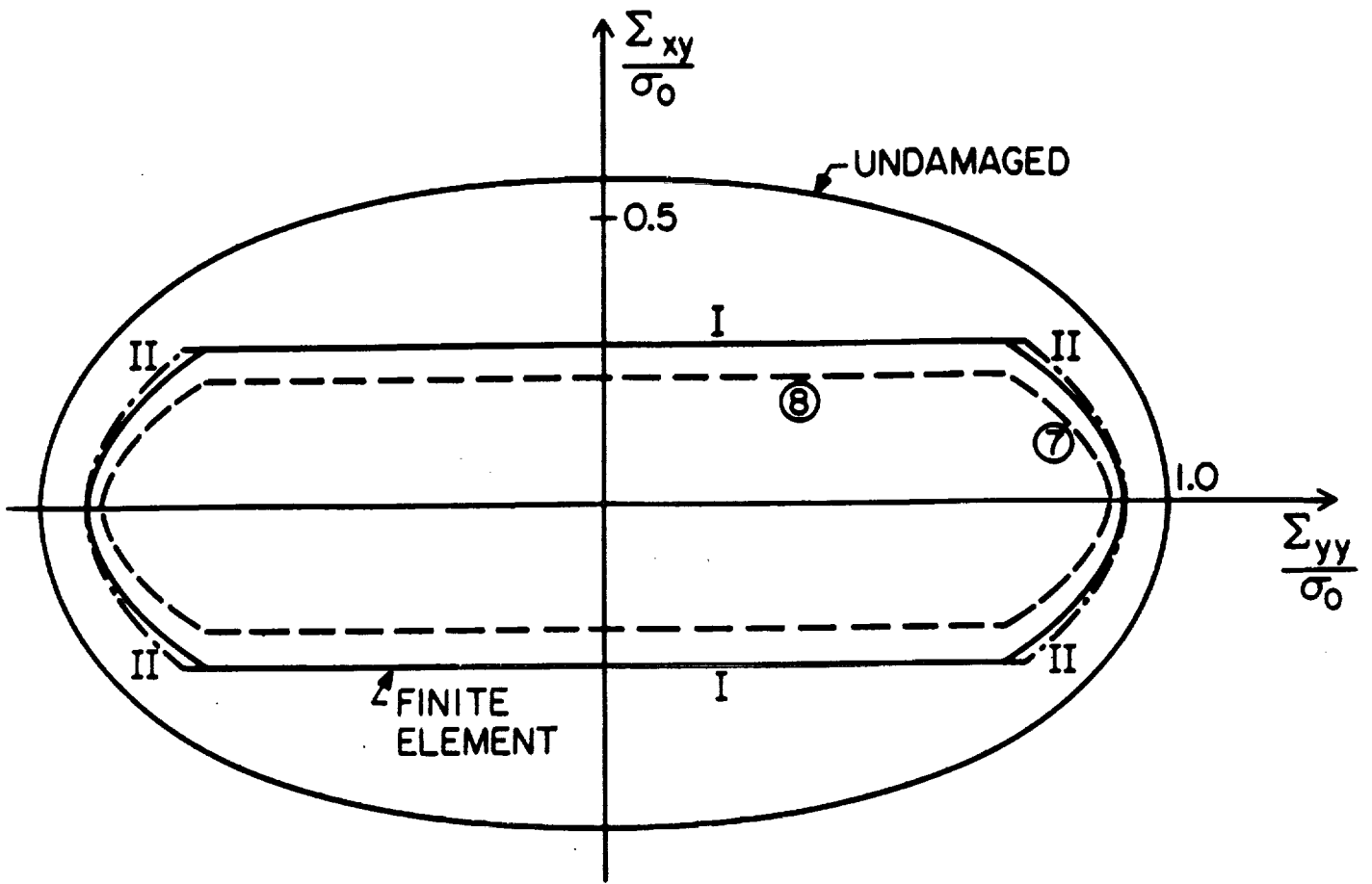


Fig. A.4 Comparison of Calculation and Approximate Limit Surface in Σ_{yy}, Σ_{xy} plane.

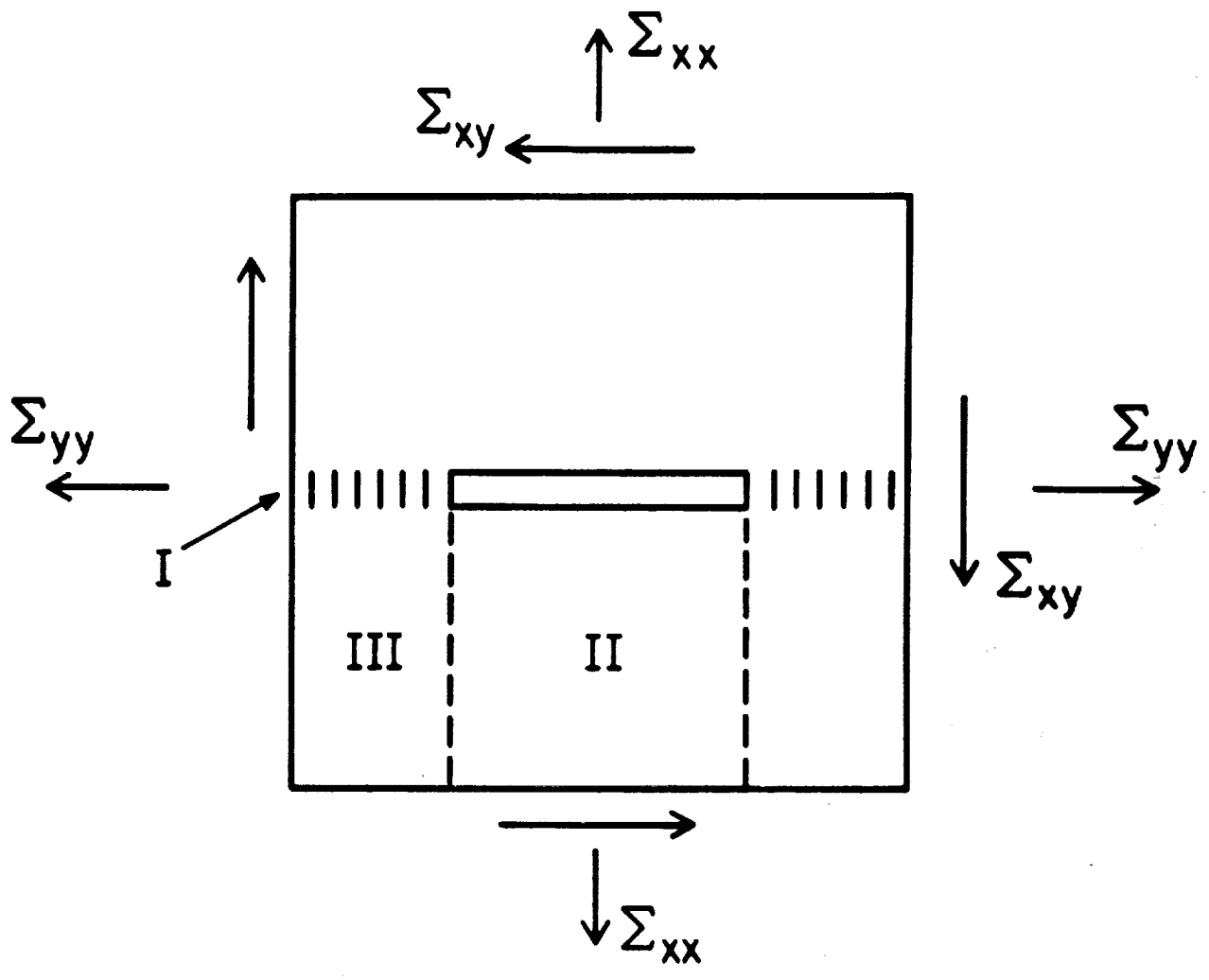


Fig. A.5 Critical Failure Fields

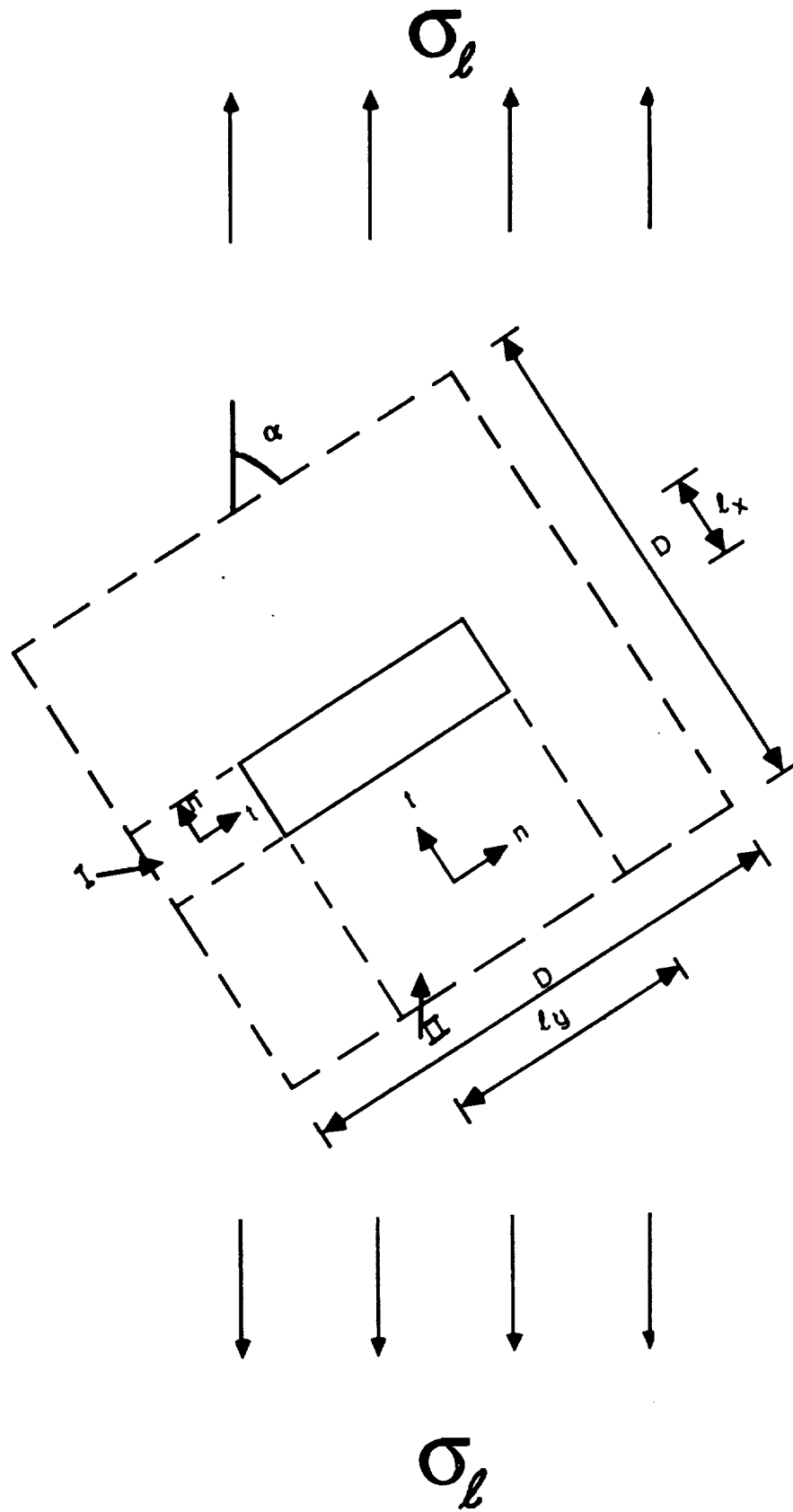


Fig. A.6 Model for simplified analysis of stress and strain at load maximum.



Report Documentation Page

1. Report No. NASA CR-185303		2. Government Accession No.		3. Recipient's Catalog No.	
4. Title and Subtitle Materials With Periodic Internal Structure: Computation Based on Homogenization and Comparison With Experiment				5. Report Date October 1990	
				6. Performing Organization Code	
7. Author(s) S. Jansson, F.A. Leckie, E.T. Onat, and M.P. Ranaweera				8. Performing Organization Report No. None	
				10. Work Unit No. 510-01-01	
9. Performing Organization Name and Address University of California Santa Barbara, California 93106				11. Contract or Grant No. NAS3-894	
				13. Type of Report and Period Covered Contractor Report Final	
12. Sponsoring Agency Name and Address National Aeronautics and Space Administration Lewis Research Center Cleveland, Ohio 44135-3191				14. Sponsoring Agency Code	
15. Supplementary Notes Project Manager, Steven M. Arnold, Structures Division, NASA Lewis Research Center.					
16. Abstract <p>The combination of thermal and mechanical loading expected in practice means that constitutive equations of metal matrix composites must be developed which deal with time-independent and time-dependent irreversible deformation. Also, the internal state of composites is extremely complicated which underlines the need to formulate macroscopic constitutive equations with a limited number of state variables which represent the internal state at the micro level. One available method for calculating the macro properties of composites in terms of the distribution and properties of the constituent materials is the method of homogenization whose formulation is based on the periodicity of the substructure of the composite. In this study a homogenization procedure has been developed which lends itself to the use of the finite element procedure. The efficiency of these procedures, to determine the macroscopic properties of a composite system from its constituent properties, has been demonstrated utilizing an aluminum plate perforated by directionally oriented slits. The selection of this problem is based on the fact that, i) extensive experimental results exist, ii) the macroscopic response is highly anisotropic and iii) that the slits provide very high stress gradients (more severe than would normally be found in practice) which severely test the effectiveness of the computational procedures. Furthermore, both elastic and plastic properties have been investigated so that the application to practical systems with inelastic deformation should be able to proceed without difficulty. The effectiveness of the procedures have been rigorously checked against experimental results and with the predictions of approximate calculations. Using the computational results it is illustrated how macroscopic constitutive equations can be expressed in forms of the elastic and limit load behavior.</p>					
17. Key Words (Suggested by Author(s)) Homogenization; Finite element; Elastic; Elastic plastic; Perforated plates			18. Distribution Statement Unclassified - Unlimited Subject Category 39		
19. Security Classif. (of this report) Unclassified		20. Security Classif. (of this page) Unclassified		21. No. of pages 65	22. Price* A04